AD_____

Award Number: W81XWH-04-1-0262

TITLE: Targeting MRS-Defined Dominant Intraprostatic Lesions with Inverse-Planned High Dose Rate Brachytherapy

PRINCIPAL INVESTIGATOR: Jean Pouliot, Ph.D.
I-Chow Hsu, M.D.
John Kurhanewicz, Ph.D.
Sue Noworelski, Ph.D.

CONTRACTING ORGANIZATION: University of California
San Francisco, California 94143-0962

REPORT DATE: February 2007

TYPE OF REPORT: Final

PREPARED FOR: U.S. Army Medical Research and Materiel Command
Fort Detrick, Maryland 21702-5012

REPORT DOCUMENTATION PAGE

Form Approved
OMB No. 0704-0188

1. REPORT DATE *(DD-MM-YYYY)*	**2. REPORT TYPE**	**3. DATES COVERED** *(From - To)*
01-02-2007	Final	26 Jan 2004 – 25 Jan 2007

4. TITLE AND SUBTITLE

Targeting MRS-Defined Dominant Intraprostatic Lesions with Inverse-Planned High Dose Rate Brachytherapy

5a. CONTRACT NUMBER

5b. GRANT NUMBER
W81XWH-04-1-0262

5c. PROGRAM ELEMENT NUMBER

6. AUTHOR(S)

Jean Pouliot, Ph.D.; I-Chow Hsu, M.D.; John Kurhanewicz, Ph.D. and Sue Noworelski, Ph.D.
E-Mail: pouliot@radonc17.ucsf.edu

5d. PROJECT NUMBER

5e. TASK NUMBER

5f. WORK UNIT NUMBER

7. PERFORMING ORGANIZATION NAME(S) AND ADDRESS(ES)

University of California
San Francisco, California 94143-0962

8. PERFORMING ORGANIZATION REPORT NUMBER

9. SPONSORING / MONITORING AGENCY NAME(S) AND ADDRESS(ES)
U.S. Army Medical Research and Materiel Command
Fort Detrick, Maryland 21702-5012

10. SPONSOR/MONITOR'S ACRONYM(S)

11. SPONSOR/MONITOR'S REPORT NUMBER(S)

12. DISTRIBUTION / AVAILABILITY STATEMENT
Approved for Public Release; Distribution Unlimited

13. SUPPLEMENTARY NOTES

14. ABSTRACT

During these three years, we have obtained CHR approval (December 2004)from the three step process (G.U., P.R.C. and C.H.R.) committees at UCSF. D.O.D. CHR approval was finally obtained in December 2006. Patient enrollment will begin immediately after receiving UCSF-CHR re-confirmation. We have developed a deformable image registration method to improve the quality of registration of (probe-in) MRSI data for (probe-out) radiation treatment planning. A similarity index (SI) of 98.1 % was obtained for rigid probe patient data. We have also obtained a class solution for the boost of DIL defined by MRI/MRSI, as well as for the sparing of organs at risk including bladder, rectum, urethra and penile bulb. Patients enrollment will be initiated shortly.

15. SUBJECT TERMS
magnetic resonance spectroscopy, Inverse planning HDR Brachytherapy

16. SECURITY CLASSIFICATION OF:			**17. LIMITATION OF ABSTRACT**	**18. NUMBER OF PAGES**	**19a. NAME OF RESPONSIBLE PERSON**
a. REPORT	**b. ABSTRACT**	**c. THIS PAGE**			USAMRMC
U	U	U	UU	42	**19b. TELEPHONE NUMBER** *(include area code)*

Table of Contents

INTRODUCTION

Research Project Description

Men with prostate cancer, in particular those with advanced local disease, benefit from dose escalation. The main objective of the DOD-PC-030909 is to exploit the ability of Magnetic Resonance Imaging combined with Magnetic Resonance Spectroscopy imaging (MRI/MRSI) to identify cancer regions within the prostate and to target those regions with a higher tumor burden with higher dose without compromising the dose coverage of the prostate and the protection to the urethra, rectum and bladder for prostate cancer patients treated with HDR brachytherapy.

The feasibility of a comprehensive approach that incorporates MRI/MRSI (anatomical and functional imagining) into the HDR brachytherapy treatment planning has been demonstrated. Using the inverse planning program IPSA, dose escalation of target regions with a higher tumor burden can be performed without increasing the dose to critical normal structures. This will be the first trial using both MR imaging and functional imaging MRSI for HDR brachytherapy planning.

Three main tasks were identified to fulfill the aims of this project:

Task 1: To determine the need for alignment and to establish alignment methods for MRI/MRSI data to HDR brachytherapy treatment planning MRI and CT images. (Months 1-24).

Task 2: To elaborate class solutions (a set of optimization constraints) appropriate for DIL boosts of the order of 150% of the prescribed dose and protection for the penile bulb and the neuro-vascular bundle valid for 90% of the cases (Months 1-12).

Task 3: To perform feasibility and short-term measures of improved effectiveness and decreased side effects of performing the proposed treatment planning protocol in a small cohort of patients (Months 18-36).

The Information provided in this third annual (final) report supports the following:

Task 1:	Months 1-24	**Completed**, (except for alignment of the non-endorectal MR images to the treatment planning CT, pending patient enrollment)
Task 2:	Months 1-12	**Completed**
Task 3:	Months 18-36	Not yet initiated

C.H.R. Approval Process Time Table

The PC-030909 grant officially opened on February 2004. A lot of effort and time were devoted by the P.I. and Co-P.I. at applying and obtaining approval from the various committees at UCSF. During the first year, we sequentially applied and successfully received approvals from the UCSF Genito-Urinary Committee (GU, March 2004), the UCSF Protocol Review Committee (PRC, July 7th, 2004), and the UCSF Committee on Human Research (CHR, approval number H11386-24294-01, December 17th, 2004). Immediately after receiving the CHR approval, the complete package was submitted to the DOD CHR for final approval. This approval was received on December 2006. Patients enrollment will begin immediately after receiving UCSF CHR Committee re-confirmation (expected for May 2007).

Research activities (Present and Future)

In the last three years, a number of research activities related to the Tasks described in the Statement of Work of the proposal have been performed. In particular, Task 1 has been accomplished during year 1 and published on the journal “Medical Physics”, and Task 2 has been accomplished during year 2 and submitted for publication. Specific details were provided in the first two annual reports. A Postdoctoral Fellow (Yongbok Kim, Ph.D.) continued to perform the work until March 2006. We have requested a no-cost extension and the research will proceed with patients enrollments as described in the research protocol.

BODY SECTION

MRI/MRSI is used to differentiate between normal and malignant prostate and define cancer-validated Dominant Intra-prostatic Lesions (DIL). A retrospective study was first conducted using data from 15 HDR patients with MRI/MRSI defined DIL. For each patient, MRSI data was first fused on the axial T2-weighted MR images. Using the prostate anatomy, the combined MRI/MRSI images were then registered on HDR planning axial CT or MR images. Targets, organs at risk and DIL were segmented. Dose constraints parameters were adjusted to define a class solution for a DIL-boost plan under the dosimetric requirements of the RTOG-0321 protocol. To determine a maximum attainable level of DIL-boost for each patient, our inverse planning dose optimization algorithm (called IPSA) was used to generate dose distributions for five different levels of DIL-boost, at least 110%, 120%, 130%, 140% and 150% of the prescribed dose. Dose volume histograms of the target and each organ at risk were compared with optimized plans without DIL boost.

On the cohort of 15 patients, dose escalations of the MRI/MRSI defined DIL were achieved in the range of 120% to 150% of the prescription with only an average of 1% increase of the V50 bladder dose, and 1 to 3% rectum depending on the boost level. Dose to the whole prostate, with the exception of the DIL, did not change. All dose limits complied with RTOG dosimetric requirements. This is accomplished by using inverse treatment planning software that can focus normally occurring high dose regions within the target volume to coincide with the DIL. Combined CHR approval from our institution and from DOD is expected early 2007 and patients enrollment will be initiated soon.

In the previous annual reports, we have described the research accomplishments related to the three following topics:

- Endorectal coil probes for prostate MRI: Assessments of tissue distortions and image alignments
- Registration of MR prostate images with biomechanical modeling and nonlinear parameter estimation
- Class solution for Inverse Planning for Dose Escalation of Dominant Intraprostic Lesions

In the last year, we have finalized the work on the establishment of Class Solutions and established the correct registration procedure between the MRSI and planning MRI/CT images.

KEY RESEARCH ACCOMPLISHMENTS

Class solution for Inverse Planning

- The class solution was obtained for the DIL-boost as well as the sparing organs at risk, including bladder, rectum, urethra and penile bulb.

MRS/MRI - planning MRI Registration protocol for Planning purpose

- A double registration procedure was established to bring on a same image the initial MR image, the MR spectroscopy information and the planning image dataset.

REPORTABLE OUTCOMES

Peer-reviewed Publications

1) Inverse Planning For HDR Prostate Brachytherapy Use to Boost Dominant Intra-Prostatic Lesion Defined by Magnetic-Resonance Spectroscopy Imaging.
Pouliot, J., Kim, Y., Lessard E., Hsu, I-C. Vigneron D. and Kurhanewicz, J. Int. J. Radiation Oncology Biol. Phys. 59 (4) 1196-1207; 2004.
The results of this paper constituted the proof of principle presented to DOD to obtain the grant

2) Endorectal and rigid coils for prostate MRI: Impact on prostate distortion and rigid image registration.
Kim Y., Noworolski S.M., Pouliot J., Hsu I.C. and Kurhanewicz J.,, Med. Phys. 32(12); 3569-3578, 2005.
Publication is provided

3) Kim Y., Hsu I.C., Lessard E., Kurhanewicz J.,, Noworolski S.M. and Pouliot J., **Class solution in inverse planned HDR prostate brachytherapy for dose escalation of DIL defined by combined MRI/MRSI**, Int. J. Radiation Onc. Biol. Phys. 2006
We have responded to the initial reviewers comments. The paper is undergoing the second round of review. Publication is provided

4) Registration of MR prostate images with biomechanical modeling and nonlinear parameter estimation
Alterovitz R., Goldberg K., Pouliot J., Hsu I.C., Kim Y., Noworolski S.M., and Kurhanewicz J.,, Med. Phys. 33(2), 446-454; 2006.
This work is directly related to present work (Task 1) but not supported by DOD -PC030909.

Presentations at International Conferences

Inverse planning in Brachytherapy: HDR and LDR, VI Last Generation Radiotherapy Course, São Paulo, Brazil, Oct. 19, 2006.

Principles and Clinical Applications of IPSA; Nucletron International Physics Seminar, Vaals, Netherlands, Sept 13-16, 2006.

IPSA, optimization in Brachythetrapy, Basis and Principles, 4ième sémnaire francophone de curiethérapie, Arcachon, France, June 15th, 2006.

Clinical experience with IPSA for prostate cancer treatment in HDR Brachytherapy, 4ième séminaire francophone de curiethérapie, Arcachon, France, June 15, 2006.

Advanced Technologies: Functional Imaging, IMRT and IGRT, NZIMRT – AIR Annual meeting, Aukland, New Zealand, August 27th, 2005.

Inverse planning for dose optimization in Brachytherapy, Institut Gustave-Roussy, Paris, France, June 28, 2004.

Presentations at National Meetings

New advances in Brachytherapy Physics, 27th Annual Meeting of American Brachytherapy Society, Philadelphia, May 12, 2006.

Advanced 3D Planning in Brachytherapy, AAPM-ABS summer school, Seattle July 18-23, 2005.

Analysis of prostate deformation due to different MRI/MRS endorectal coils for image fusion and brachytherapy treatment planning. Med. Phys.31 (6); 1728-1728, 2004 (Abstract).

Dose Constraints in Inverse Planning HDR Prostate Brachytherapy for The Dose Escalation of DIL Defined by MR Spectroscopy Imaging. *Annual Meeting of the American Brachytherapy Society*, San Francisco 2005.

Future Presentations at National and International Conferences

Dose escalation using functional imaging, 12th International Conference Optimal Use of Advanced Radiotherapy in Multimodality Oncology, Rome, Italy, 20th to 23rd June 2007.

Advances in Optimization Strategies, Physics Symposium, Int. Society for Therapeutic Radiology and Oncology, Joint GEC-ESTRO-ISIORT Meeting, Montpellier, May 9-12, 2007.

Dose Escalation of Dominant Intra-Prostatic Lesion Defined by Magnetic-Resonance Spectroscopy Imaging Using Inverse Planning for HDR Prostate Brachytherapy,DOD-PCRP- Meeting, Innovative Minds in Prostate Cancer Today (IMPaCT), Atlanta Georgia, Sept. 5-8, 2007. (Abstract submitted for presentation).

DETAILS OF REPORTABLE OUTCOMES

The details of the previous reportable outcomes were provided in the two previous annual reports as well as in the publications provided in Appendices. References cited in the publications (published or in press) support our experimental objectives, choices made in experimental design, and interpretation of results.

Class solutions

A class solution was developed for dose escalation of a DIL defined by combined MRI/MRSI in inverse planned HDR prostate brachytherapy. Using the class solution, a certain level of DIL-boost is feasible for some patients under RTOG-0321 dosimetric requirements depending on rectal and bladder doses. While the target dose was slightly increased, the DIL dose was noticeable enhanced (on average, 82% of the DIL volume could receive 150% of the prescribed dose) without any violation of the dosimetric requirements. With further adjustment of the class solution, the DIL could be boosted by 150 – 150 for 13 out of 15 patients while satisfying dosimetric requirements. Hence, the established class solution for a DIL-boost is a good starting point to explore a customized HDR prostate brachytherapy plan for a specific patient.

Registration procedure between the MRSI and planning MRI/CT images

A double registration procedure was established to bring on a same image the initial MR image, the MR spectroscopy information and the planning image dataset. The MRI/MRS registration procedure resulting on an MR image with defined validated cancer areas (Figure in the center) was established and reported in year 2. A procedure to adapt the format of this combined MRI/ MRS image into DICOM was finalized this year. This allows to import the image in the planning software. The planning image showing the current anatomy and the catheters can then be registered with the combined MRI/MRS image, providing all the anatomical information in the same reference system (Figure, right).

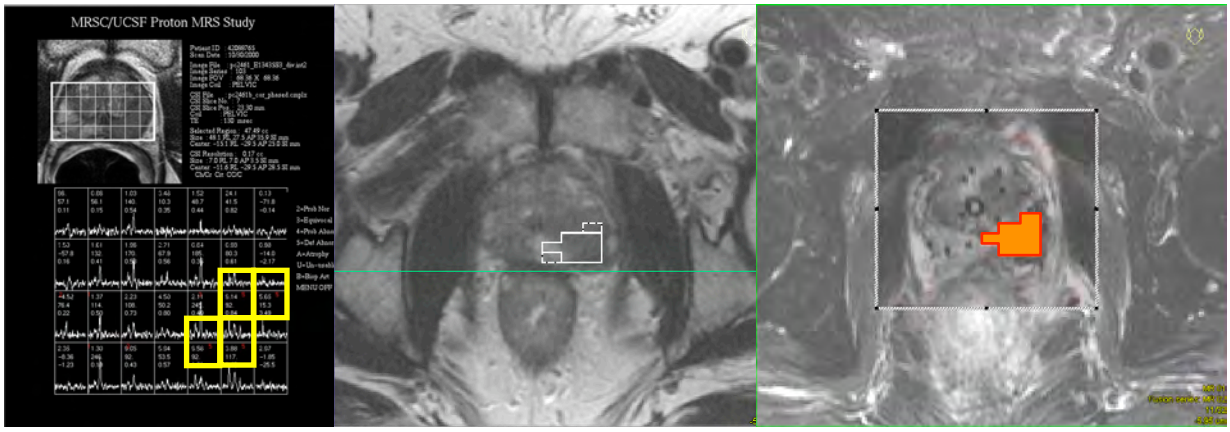

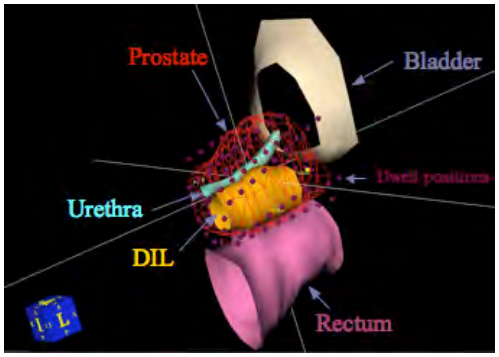

Multiple contours (Figure right) based on anatomical and spectroscopic information result on the clinical target, the DIL and the organs at risk, bladder, urethra, rectum and bulb. Then catheters are digitally reconstructed. The optimization routine IPSA is called, and using the class solution already defined, produces a dose distribution that tightly conform to the target, boost the DIL and spare the organs at risk.

All the procedures and methodology have been developed and are ready to be used clinically. As it was mentioned previously, the enrollment of patients will be initiated shortly, as soon as the final CHR approval is obtained. We expect to initiate the protocol in June 2007.

LIST OF ACRONYMS

CHR: Committee on Human Research
CT: Computed Tomography
DIL: Dominant Intraprostatic Lesion
S/I: Superior-Inferior
R/L: Right-Left
A/P: Antero-Posterior
DOD: Department of Defense
ERC: Endo-Rectal Coil
GU: Genito-Urinary Committee
HDR: High Dose-Rate
IPSA: Planning with Simulated Annealing
MRI: Magnetic Resonance Imaging
MRSI: Resonance Spectroscopy Imaging
PRC: Review Committee
ROI: Region of Interest
RTOG: Radiation Therapy Oncology Group
UCSF: University of California California, San Francisco
DIL: Dominant Intra-prostatic Lesion
CG: Central Gland
PZ: Peripheral Zone
TRUS: Trans-rectal Ultra-Sound
OAR: Organs at Risk

APPENDICE

Publications

1- Pouliot, J., Kim, Y., Lessard E., Hsu, I-C. Vigneron D. and Kurhanewicz, J. **Inverse Planning For HDR Prostate Brachytherapy Use to Boost Dominant Intra-Prostatic Lesion Defined by Magnetic-Resonance Spectroscopy Imaging.** Int. J. Radiation Oncology Biol. Phys. 59 (4) 1196-1207; 2004. (The results of this paper constituted the proof of principle presented to DOD to obtain the grant)/

2- Kim Y., Noworolski S.M., Pouliot J., Hsu I.C. and Kurhanewicz J., **Expandable and rigid endorectal coils for prostate MRI: Impact on prostate distortion and rigid image registration**, Med. Phys. 32(12); 3569-3578, 2005.

3- Kim Y., Hsu I.C., Lessard E., Kurhanewicz J.,, Noworolski S.M. and Pouliot J., **Class solution in inverse planned HDR prostate brachytherapy for dose escalation of DIL defined by combined MRI/MRSI**, in Preparation, to be submitted to Int. J. Radiation Onc. Biol. Phys. 2006.

4. Alterovitz R., Goldberg K., Pouliot J., Hsu I.C., Kim Y., Noworolski S.M., and Kurhanewicz J., **Registration of MR prostate images with biomechanical modeling and nonlinear parameter estimation**, Med. Phys. 33(2), 446-454; 2006. (related to present work but not supported by DOD -PC030909).

ABSTRACTS

Abstract: Glac-ESTRO Annual Meeting, Barcelona-2004

TARGETING DOMINANT INTRAPROSTATIC LESION USING FUNCTIONAL IMAGING WITH MR SPECTROSCOPY AND HIGH DOSE RATE BRACHYTHERAPY

J.Pouliot, Y.Kim, E. Lessard, I.C. Hsu, D.B. Vigneron and J. Kurhanewicz

The high specificity of Magnetic Resonance Spectroscopy Imaging (MRSI) to metabolically identify cancer can be used to improve the ability of MRI to detect the location and extent of cancer within the prostate. In this work, we evaluate the feasibility of using MRI/MRSI to identify the dominant intraprostatic lesion (DIL) and to selectively boost the lesion using inverse planned High Dose Rate (HDR) brachytherapy.

The MRI/MRSI scans were obtained on a 1.5 Tesla GE system for 10 patients in the supine position using the body coil for excitation and a pelvic phased array coil in combination with a commercially available balloon-covered expandable endorectal coil for signal reception. The locations of the DIL on the MRI/MRSI scans were manually transferred on the planning CT scans. Our inverse planning optimization algorithm (IPSA) was used to increase the dose delivered to the DIL. Three values of boosts (B1, B2 and B3) were computed to establish to what extent the DIL dose can be increased without affecting the dose delivered to the organs at risk while maintaining the prostate dose coverage. Dose Volume Histograms (DVH) of the target and each organ at risk were computed and the results compared with optimized plans without DIL boost.

Combined MRI/MRSI identified two DILs in 8 of the ten patients studied, and a single DIL in the remaining two. For all boost levels, including the reference plans, the average target V100 (%) are above 96% (range 94 to 99%). The bladder V50s increase by an absolute value of about 1% for the various boost levels. The absolute increases in V50 for the rectum is less than 1% for B1 and about 3% for B2 and B3. However, the volume of the urethra receiving more than 120% of the prescribed dose is increased by 13.4% for B1 and by 32.0 and 32.5 % for B2 and B3 relatively to the reference plan, respectively. In spite of the increase due to B3, the doses that would be delivered to the urethra were still below the doses that were planed and used clinically before the clinical introduction of the inverse planning tool.

The B1 boost provided DIL dose levels to 120% with no increase of the dwell times. This is the nature of the inverse planning ability to move the hot spots where appropriate, in that case the DIL. This is inherently difficult to achieve with forward planning. Larger boost values of up to 150% will have to be investigated before their clinical use can be considered.

Abstract: 26th Annual Meeting of the American Brachytherapy Society, 2005.

DOSE CONSTRAINTS IN INVERSE PLANNING HDR PROSTATE BRACHYTHERAPY FOR THE DOSE ESCALATION OF DIL DEFINED BY MR SPECTROSCOPY IMAGING

Yongbok Kim PhD*, I-Chow J. Hsu MD*, Etienne Lessard PhD*, John Kurhanewicz PhD**, Susan Moyher Noworolski PhD**, and Jean Pouliot PhD*

*Department of Radiation Oncology, University of California, San Francisco, Comprehensive Cancer Center, 1600 Divisadero Street, San Francisco, CA 94143-1708

**The Center for Molecular and Functional Imaging, Department of Radiology, University of California, San Francisco, 185 Berry Street, Suite 350, San Francisco, CA 94143-0946

Purpose:
To obtain the dose constraint set (class solution) for the boost of dominant intraprostatic lesions (DILs) defined by MR spectroscopy imaging (MRSI) in HDR brachytherapy of the prostate cancer and the maximum achievable boost level under RTOG0321 dosimetric requirement.

Materials and Methods:
For 10 patients (A to J), DILs were manually contoured on HDR planning CT/MR images based on combined MRI/MRSI. A lesion containing at least 3 contiguous MRSI validated cancer voxels was called DIL. The class solution of dose constraints, acceptable dose range and penalty values, were obtained from our previous clinical experience on inverse planning technique (IPSA). For each patient, six plans (a without-boost and 5 different levels of dose escalation to the DILs requesting a minimum of 110, 120, 130, 140 and 150% of the prescribed dose, respectively) were generated using IPSA. Dosimetric indices for each plan were computed and compared with the requirement of RTOG0321 protocol (V100 > 90% for target coverage, V75 < 1 cc for bladder and rectum, and V125 < 1 cc for urethra) to determine the acceptable level of dose escalation.

Results:
Plans without boost satisfied all RTOG0321 requirements with average dose coverage of 92.1% to target (range from 90.6 to 93.8%). Four (B, C, D, and J) out of 10 patients prohibited any boost whereas a certain level of boost to the DILs was feasible for the rest of patients, minimum dose of 110% for patient E, 120% for patient H and I, 140% for patient A and F, and 150% for patient G, respectively. The violation of RTOG0321 protocol is rectal dose for 9 patients and bladder dose for patient C. The average benefit from maximum achievable boost for 6 patients is 1.1% increase of target coverage and 5% increase of V120 dose to DILs compared with a plan without boost.

Conclusions:
A certain level of dose escalation to DILs defined by MRI/MRSI is possible for some patients using class solution of IPSA under RTOG0321 dosimetric requirements depending on rectal and bladder dose.

The work was supported by grant from the Department of Defense Prostate Cancer Research Program (PCRP)-030909

Invited Speaker: Brachytherapy: 5(2), 2006; Special Section: 27th Annual Meeting of the American Brachytherapy Society, May 10-12, 2006.

Multi-Focal Inverse Planning Dose Optimization in Brachytherapy: Let's make Hot Spots Count.

Jean Pouliot

Comprehensive Cancer Center, University of California, San Francisco,
San Francisco, California.

Abstract (submitted for presentation)
DOD-PCRP-Meeting, Innovative Minds in Prostate Cancer Today (IMPaCT)
Atlanta Georgia, Sept. 5-8, 2007.

DOSE ESCALATION OF DOMINANT INTRA-PROSTATIC LESION DEFINED BY MAGNETIC-RESONANCE SPECTROSCOPY IMAGING USING INVERSE PLANNING FOR HDR PROSTATE BRACHYTHERAPY

Jean Pouliot; I-Chow Hsu; Etienne Lessard; Yongbok Kim; (Comprehensive Cancer Center, University of California, San Francisco, San Francisco, California) Susan Moyher Noworolski; John Kurhanewicz **(**Center for Molecular and Functional Imaging, Department of Radiology, University of California, San Francisco, San Francisco, California)

Men with prostate cancer, in particular those with advanced local disease, benefit from dose escalation. The main objective of the DOD-PC-030909 is to exploit the ability of Magnetic Resonance Imaging combined with Magnetic Resonance Spectroscopy imaging (MRI/MRSI) to identify cancer regions within the prostate and to target those regions with a higher tumor burden with higher dose without compromising the dose coverage of the prostate and the protection to the urethra, rectum and bladder for prostate cancer patients treated with HDR brachytherapy.

MRI/MRSI is used to differentiate between normal and malignant prostate and define cancer-validated Dominant Intra-prostatic Lesions (DIL). A retrospective study was first conducted using data from 15 HDR patients with MRI/MRSI defined DIL. For each patient, MRSI data was first fused on the axial T2-weighted MR images. Using the prostate anatomy, the combined MRI/MRSI images were then registered on HDR planning axial CT or MR images. Targets, organs at risk and DIL were segmented. Dose constraints parameters were adjusted to define a class solution for a DIL-boost plan under the dosimetric requirements of the RTOG-0321 protocol. To determine a maximum attainable level of DIL-boost for each patient, our inverse planning dose optimization algorithm (called IPSA) was used to generate dose distributions for five different levels of DIL-boost, at least 110%, 120%, 130%, 140% and 150% of the prescribed dose. Dose volume histograms of the target and each organ at risk were compared with optimized plans without DIL boost.

On the cohort of 15 patients, dose escalations of the MRI/MRSI defined DIL were achieved in the range of 120% to 150% of the prescription with only an average of 1% increase of the V50 bladder dose, and 1 to 3% rectum depending on the boost level. Dose to the whole prostate, with the exception of the DIL, did not change. All dose limits complied with RTOG dosimetric requirements. This is accomplished by using inverse treatment planning software that can focus normally occurring high dose regions within the target volume to coincide with the DIL. Combined CHR approval from our institution and from DOD is expected early 2007 and patients enrollment will be initiated soon.

The feasibility of a comprehensive approach that incorporates MRI/MRSI (anatomical and functional imagining) into the HDR brachytherapy treatment planning has been demonstrated. Using the inverse planning program IPSA, dose escalation of target regions with a higher tumor burden can be performed without increasing the dose to critical normal structures. This will be the first trial using both MR imaging and functional imaging MRSI for HDR brachytherapy planning.

IMPACT: This new approach will allow dose escalation to be targeted to areas of high cancer cell density. We believe these refinements of HDR brachytherapy planning will lead to new therapeutic approaches that may improve clinical results.

Expandable and rigid endorectal coils for prostate MRI: Impact on prostate distortion and rigid image registration

Yongbok Kim,[a)] I-Chow J. Hsu, and Jean Pouliot
Department of Radiation Oncology, University of California, San Francisco, Comprehensive Cancer Center, 1600 Divisadero Street, Suite H1031, San Francisco, California 94143-1708

Susan Moyher Noworolski, Daniel B. Vigneron, and John Kurhanewicz
The Center for Molecular and Functional Imaging, Department of Radiology, University of California, San Francisco, 185 Berry Street, Suite 350, San Francisco, California 94143-0946

(Received 7 February 2005; revised 20 September 2005; accepted for publication 20 September 2005; published 15 November 2005)

Endorectal coils (ERCs) are used for acquiring high spatial resolution magnetic resonance (MR) images of the human prostate. The goal of this study is to determine the impact of an expandable versus a rigid ERC on changes in the location and deformation of the prostate gland and subsequently on registering prostate images acquired with and without an ERC. Sagittal and axial T_2 weighted MR images were acquired from 25 patients receiving a combined MR imaging/MR spectroscopic imaging staging exam for prostate cancer. Within the same exam, images were acquired using an external pelvic phased array coil both alone and in combination with either an expandable ERC (MedRad, Pittsburgh, PA) or a rigid ERC (USA Instruments, Aurora, OH). Rotations, translations and deformations caused by the ERC were measured and compared. The ability to register images acquired with and without the ERC using a manual rigid-body registration was assessed using a similarity index (SI). Both ERCs caused the prostate to tilt anteriorly with an average tilt of 18.5° (17.4±9.9 and 19.5±11.3°, mean±standard deviation, for expandable and rigid ERC, respectively). However, the expandable coil caused a significantly larger distortion of the prostate as compared to the rigid coil; compressing the prostate in the anterior/posterior direction by 4.1±3.0 mm vs 1.2±2.2 mm (14.5% vs 4.8%) ($p<0.0001$), and widening the prostate in the right/left direction by 3.8±3.7 mm vs 1.5±3.1 mm (8.3% vs 3.4%) ($p=0.004$). Additionally, the ability to manually align prostate images acquired with and without ERC was significantly ($p<0.0001$) better for the rigid coil (SI=0.941±0.008 vs 0.899±0.033, for the rigid and expandable coils, respectively). In conclusion, the manual rigid-body alignment of prostate MR images acquired with and without the ERC can be improved through the use of a rigid ERC. © *2005 American Association of Physicists in Medicine*. [DOI: 10.1118/1.2122467]

Key words: expandable endorectal coil, rigid endorectal coil, prostate distortion, rigid image registration, MRI

I. INTRODUCTION

Recent studies have demonstrated that the detection and characterization of prostate cancer can be improved by combining the anatomic and metabolic information provided by magnetic resonance imaging (MRI) and magnetic resonance spectroscopic imaging (MRSI).[1–8] The combined prostate MRI and MRSI exam can be performed in less than an hour using a standard clinical 1.5 T MRI scanner and commercially available coils, and MR vendors are offering or are close to releasing product versions of this exam. An expandable endorectal coil[9] (ERC) integrated into a pelvic phased array coil is commonly used for signal reception in the MRI/MRSI prostate exam due to the improved signal-to-noise ratio (SNR) and better spatial resolution MR images obtained as compared to using pelvic phased array coils alone.[3–5] The ERC is also critical for the acquisition of high spatial resolution (≈0.3 cm^3) MRSI data of the prostate due to the approximate tenfold increase in SNR over the prostate provided by the ERC relative to external phased array coils.[9]

Several recent studies have utilized MRI/MRSI data to identify the dominant regions of cancer inside the prostate for improved radiation treatment planning.[10–14] In particular, we used MRI/MRSI to escalate dose to selected regions inside the prostate without compromising the dose coverage of the prostate and the protection of the organs at risk for patients treated with high dose rate brachytherapy.[12] However, the displacement and distortion of the prostate caused by the ERC used in staging MRI/MRSI exams cause difficulties with alignment of the MRI/MRSI data to treatment planning computed tomography (CT) or MRI images which are typically acquired without an ERC or to transrectal ultrasound planning images that employ an endorectal probe having a different shape. In addition to the commercially available expandable ERC, a number of rigid ERCs have also been designed and used for imaging and spectroscopic studies of the prostate.[6–8] The goal of this study is to determine the impact of the commonly used expandable ERC versus a rigid alternative ERC on changes in location and deformation of

the prostate gland and subsequently on registering prostate images acquired with and without these ERCs.

II. METHODS AND MATERIALS

A. Patients cohorts

Twenty biopsy proven prostate cancer patients clinically referred for a combined MRI/MRSI staging exam between January and July of 2003 were studied. Five additional patients were enrolled between May and June of 2005 and therefore the total number of patients for this study was 25. The study was approved by our Committee on Human Research and informed consent was obtained from all patients. The patients had a mean Gleason score of 6.9 (6.6 for the rigid ERC patients versus 7.4 for the expandable ERC patients) and a mean age of 66 for each ERC group. The average volumes of the prostates were 31.4 cm^3, with a range from 15.1 to 47.7 cm^3 for rigid ERC patients, and 42.3 cm^3, with range from 14.8 to 91.8 cm^3 for expandable ERC patients. There were two large prostates, at 63.5 cm^3 for patient Q and 91.8 cm^3 for patient R. If the two patients with large prostates in the expandable ERC patient group are excluded, the mean prostate volume for the remaining eight patients is 33.5 cm^3, similar to the rigid ERC patient group.

B. MRI protocol

Combined MRI/MRSI was obtained using either a rigid ERC (15 studies, referred to as A to O, USA Instruments, Aurora, OH) or an expandable ERC (10 studies, referred to as P to Y, MedRad, Pittsburgh, PA) in combination with an external phased array of coils on a 1.5 T GE system (Signa, GE Medical Systems, Milwaukee, WI). For rigid coil cases, the USA torso phased array was used, while the GE pelvic phased array was used for the expandable coil cases. These two ERCs were selected as the MedRad coil is the only MR ERC currently available commercially and the USA Instruments ERC is commercially manufactured and will soon be a commercially available alternative ERC. Initially, no particular selection process was used to assign subjects to a coil configuration. During the course of this study, it was discovered that the rigid ERC gave less distortion than the expandable ERC and thus the rigid ERC became the coil used for all our radiation treatment planning prostate imaging examinations. Due to this protocol decision, initially only five subjects were studied with the expandable ERC, whereas an additional ten, totaling 15, were studied with the rigid ERC. To improve comparison between the ERCs, an additional five subjects were studied with the expandable ERC, making the final numbers 15 for the rigid ERC and ten for the expandable ERC.

The expandable coils, at 44 mm right/left (R/L) by 79 mm superior/inferior (S/I), were larger than the rigid coils at 22.5 mm R/L by 65 mm S/I. The probes themselves also differed in size and shape. The expandable ERC had a circular cross section, once inflated, with a 48 mm diameter. The rigid probe was a half ellipse, with the anterior surface flat. Its R/L extent was 29 mm and its anterior/posterior (A/P) extent was 16.5 mm. The S/I length of the expandable ERC probe (86 mm) was also longer than the rigid probe (82 mm).

The ERC images used in this study were acquired during a "PROSE" MRI/MRSI staging exam (GE Medical Systems, Milwaukee, WI).[15] The details of the MR imaging technique have been previously described.[12,16–18] In brief, patients were examined in the supine position, using the body coil for excitation and a combination of the ERC and pelvic phased array for signal reception. Thin-section high spatial resolution axial, coronal and sagittal T_2 weighted fast spin-echo images of the prostate and seminal vesicles were obtained using the following parameters: TR(time of repetition)/effective TE(time of echo)=5000/96 msec, echo train length=16, slice thickness=3 mm, inter-slice gap=0 mm, field of view (FOV)=14 cm, matrix 256×192, frequency direction antero-posterior (to prevent obscuration of the prostate by ERC motion artifact), and three excitations. The ERC was removed at the end of the staging MRI/MRSI exam with the subject remaining on the imaging table. Additional sagittal and axial fast spin echo T_2 weighted images were acquired without the ERC using the phased array coil alone for signal reception. As with the ERC, patients were scanned in the supine position. All imaging acquisition parameters were the same as for the ERC images except for increasing the FOV to 16 cm in order to compensate for the reduction in SNR obtained without the use of an ERC.

C. ERC induced changes in prostate location and shape

To assess the effect of the ERCs on the location and shape of the prostate, R/L, A/P, and S/I lengths and positions of the prostate were measured. Measurements were obtained on the MR images acquired with and without an ERC. The user modified the image intensity (window/level) settings to best depict the anatomy in question. Such settings were not consistent within or across subjects due to the differences in signal of the images obtained with an ERC versus without and due to inter-patient variability. Prior to two-dimensional (2D) image registration, the MR images acquired with and without the presence of ERCs were rotated to align the data into the same plane, approximately perpendicular to the long (superior-inferior) axis of the prostate. The amount of rotation was determined by the difference between the series angle and the prostate angle. The prostate angle was defined as the angle (θ) between the line perpendicular to the axis of magnet bore and the long axis (S/I direction) of the prostate. The axial T_2 weighted prostate images in this study were often acquired obliquely in the S/I dimension in order to obtain true axial images through the prostate, and needed to be accounted for when calculating the prostate angle. This oblique angle was referred to as the series angle and was obtained from the series image header. The prostate angle was determined using T_2 weighted sagittal MR images taken at the middle of the prostate (Fig. 1). Three approaches (I, II and III) were used to draw a line along the superior-inferior direction of the prostate in order to define a long axis (S/I

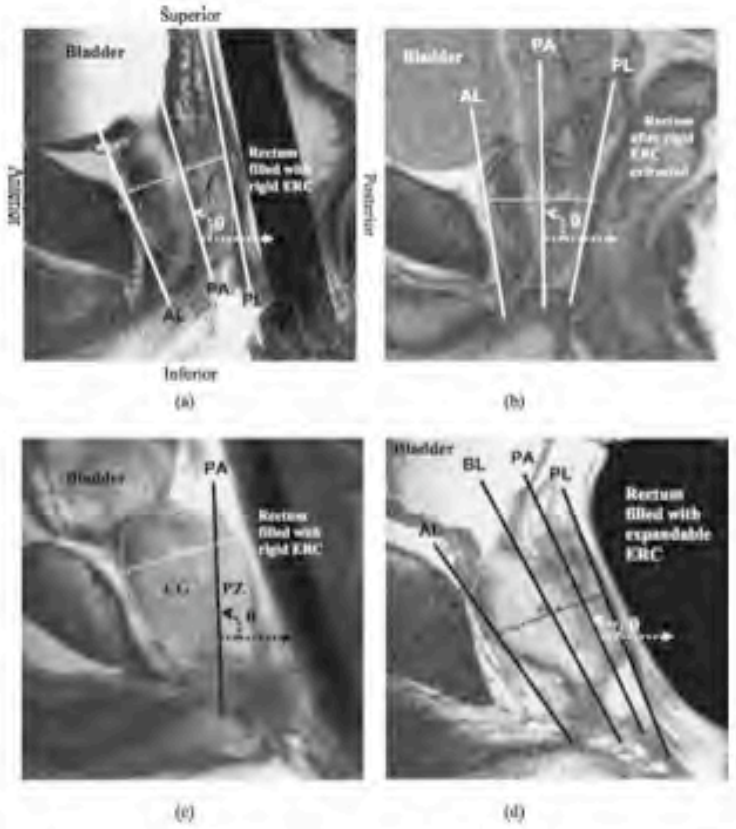

FIG. 1. T_2 weighted sagittal MR images illustrating the three approaches used to determine the prostate angle: Approach I was used for (a) and (b), Approach II for (c), and Approach III for (d). The anterior/posterior (A/P) distance (dashed line in the A/P direction) was 2.96, 3.22, 3.45, and 2.71 cm for (a), (b), (c), and (d), respectively. The prostate angle (θ, curved dashed arrow) was measured counterclockwise between the prostate S/I axis (PA) and the line perpendicular to the axis of magnet bore (expressed with a dot straight arrow). The prostate angle was 106.1, 90.2, 91.5 and 114.5° for (a), (b), (c) and (d), respectively. In (a), (b), and (d), the straight line along the anterior and posterior surface of the prostate is defined as AL and PL, respectively. In (c), CG and PZ stand for central gland and peripheral zone of the prostate. In (d), BL means the bisector line between AL and PL.

direction) of the prostate, and thus, the prostate angle. Three approaches were necessary due to the inability to clearly visualize the anterior and posterior surfaces of the prostate, the surgical pseudo capsule and/or when there were dramatic changes in the A/P width of the prostate between the ERC in and ERC out acquisitions.

The three approaches use different methods to determine the long axis of the prostate. The angle between this line and the line perpendicular to the axis of magnet bore is then calculated as the prostate angle. Approach I worked for 17 out of the 25 studies (12 out of 15 for rigid ERCs and 5 out of 10 for expandable ERCs). In this approach, the long axis of the prostate was simply calculated based on drawing straight lines along the posterior and anterior surfaces of the prostate and determining the bisector of these lines (i.e., the average of the two angles) [Figs. 1(a) and 1(b)]. Approach II was used for six studies (patients E, N, O for rigid ERCs and Q, R, U for expandable ERCs). In these cases, there was a greater than 10% increase in the A/P dimension of the prostate causing a large difference in the prostate angle determined using lines drawn along the posterior and anterior surfaces of the prostate. However, in these cases, the surgical pseudo capsule which separates the central gland from the peripheral zone was well visualized and a line drawn along the surgical pseudo capsule could be used to define the long axis of the prostate [Fig. 1(c)]. In the remaining two cases (patients P and T for expandable ERC), there was a more than 10% increase in the A/P dimension and the surgical pseudo capsule was not well visualized. In these cases (Approach III), the long axis of the prostate was calculated based on the average of the angle formed by the bisector of the anterior and posterior lines and the angle determined by the posterior line [Fig. 1(d)]. In each patient, the same approach was always taken for the case with an ERC and the case without an ERC. It is recognized that the three approaches may determine a different absolute angle, as they are based on different anatomical landmarks. However, the intent was to determine a procedure to consistently calculate the difference in rotation of the prostate when imaged with an ERC versus without an ERC. To evaluate the effect of the different approaches, all three approaches were performed in the patients for whom Approach I was possible.

In order to assess the change in position and shape of the prostate caused by the expandable and rigid ERCs, rotation in the sagittal plane (Rot_{Sag}), and translations ($T_{R/L}, T_{A/P}, T_{S/I}$), and deformations ($D_{R/L}, D_{A/P}, D_{S/I}$) along the R/L, A/P and S/I dimensions were determined. Rotations of the prostate in coronal and axial planes (Rot_{Cor}, Rot_{Axi}) were visually negligible. Changes in the prostate angle on ERC-in versus ERC-out cases were calculated and statistically compared for the ERCs (rigid and expandable) using a

nonparametric test, Wilcoxon matched-pairs signed-rank test, and were subsequently used to rotate the prostate during image alignment.

The translations in the R/L and A/P dimensions ($T_{R/L}$, $T_{A/P}$) were measured in the axial plane since image registration between studies was performed in the axial plane. The translation in the S/I dimension ($T_{S/I}$) was determined by selecting a ERC-in axial MR image showing the same anatomy (ejaculatory ducts, urethra, benign prostatic hyperplasia nodules) as a ERC-out axial MR image.

Deformation of the prostate in the R/L and A/P dimensions ($D_{R/L}$, $D_{A/P}$) was determined by manually measuring the maximum R/L and A/P distances of the prostate between axial images acquired with and without the ERC. Two edge points of the prostate in both the approximate R/L and approximate A/P dimensions were visually selected to measure the maximum extent of the prostate in the R/L and A/P dimensions. Hence, sometimes the maximum R/L and A/P measures of the prostate were not perfectly perpendicular, as in Figs. 3(c) and 3(d), although in general they were perpendicular to each other. The deformation of the prostate in the S/I dimension ($D_{S/I}$) was measured using the total number of axial images containing the prostate acquired with and without the ERC. Since deformation visually changed along the length of the prostate, separate deformation measurements were made using axial images taken from the prostatic base, midgland and apex.

D. Image registration

The ability to register images acquired with and without the ERC was determined using a manual rigid-body registration and assessed using a similarity index (SI).[19,20] Two independent observers did the contouring and registration process for all patients to assess inter-observer differences on the calculated SI. To accomplish this, the contour of the prostate was manually drawn on each contiguous 2D axial MR image forming a three-dimensional (3D) volume that was aligned between images acquired with and without the ERC. Prior to contouring the prostate, the contiguous 2D MR images were stacked together to form a 3D volume, and the volume was rotated in the sagittal plane by the difference in prostate angle after accounting for the series angle (Rot_{sag} = (MRI series angle − prostate angle)$_{ERC\text{-}in}$ − (MRI series angle−prostate angle)$_{ERC\text{-}out}$). Subsequently, the resolution (mm/pixel) of the ERC-in MR images was changed to equal that of the ERC-out MR images and the ERC-in and ERC-out images were visually aligned in the S/I dimension based on the anatomy of the prostate. Finally, contours were manually drawn on the 2D images outlining the prostate, and the contoured ERC-in volume was translated in the R/L and A/P directions, based on the mean value of the R/L and A/P coordinates of the contoured ERC-out volume.

The exactness of image registration between ERC-in and ERC-out contoured volumes was evaluated using a SI value. The SI value (ranging from 0 to 1) was defined as the ratio of twice the common area ($A \cap B$) to the sum of the individual areas ($A+B$). For example, if the contoured volumes were perfectly matched, the SI value would be 1, whereas no overlap would result in a SI value of 0.

$$SI = \frac{2\{A \cap B\}}{A+B} = \frac{2c}{a+b+2c},$$

where "A" and "B" are the two contoured volumes, "a" is the area belonging to only contour volume A, "b" is the area occupied by only contoured volume "B" and "c" is the overlapping region between volumes A and B.

III. RESULTS

A. Impact of ERC on prostate location

There were 17 cases in which the increase in A/P dimension was less than 10%, and thus, Approach I for determining the prostate angle could be applied. All three approaches described in Sec. II C were performed in these subjects and summarized in Table I. As described in the methods, these approaches measure the prostate angle differently and thus, determine different angles. For a prostate, the prostate angle is significantly different depending on which approach was employed [$p<0.0001$ by Friedman test, nonparametric repeated measures ANOVA (Analysis of variation between groups)] and, in general, the largest angle is measured by Approach I, the second by approach III ($6.4\pm3.6°$ less than Approach I), and the smallest by Approach II ($13.2\pm8.0°$ less than Approach I). The case with the largest discrepancy in measured angles had less than 30° variation among the three approaches (Table I). The prostate angles determined for each subject were used to rotate the ERC-in and ERC-out image data into the same plane. For this, the difference in angle between ERC-in and ERC-out studies is of primary relevance and was not significantly different for the three approaches ($p=0.1134$ by Friedman test). The mean±standard deviation values of the angle difference were 20.0 ± 11.4, 19.7 ± 9.8 and 21.8 ± 11.3 for Approaches I, II and III, respectively.

Figure 2 summarizes the changes in prostate angle between ERC-in and ERC-out studies for the 25 patient studies (15 rigid coil studies, and 10 expandable coil studies). As observed in Fig. 2, both ERCs [Fig. 2(a)—rigid coil, Fig. 2(b)—expandable coil] caused the superior portion of the prostate to tilt anteriorly with an average angle of 18.5°. Specifically, the mean angle change between ERC-in and ERC-out was 19.5° for the rigid coil, and 17.4° for the expandable coil.

B. Impact of ERC on prostate deformation

As can be seen in comparing Fig. 1(a) with Fig. 1(b), the presence of the rigid ERC did not affect the S/I length of prostate as compared to the images acquired without the ERC. Quantitatively, the difference in the S/I length of the prostate measured between images acquired with and without either ERC was always less than the thickness of an axial MR image (3 mm).

TABLE I. Comparison of long axes of the prostate measured by three different approaches (Approaches I, II, and III mentioned in Sec. II C) for 17 patients. Unit is degrees.

	Approach (ERC in)			Approach (ERC out)			Angle difference (ERC in)−(ERC out)		
	I	II	III	I	II	III	I	II	III
Mean	106.3	93.2	100.8	86.3	73.5	79.0	20.0	19.7	21.8
SD[a]	9.9	7.9	10.1	17.9	13.8	17.1	11.4	9.8	11.3
Median	106.1	93.7	101.8	86.6	71.3	79.6	17.7	18.8	20.6
Minimum	86.3	77.8	75.7	51.5	44.9	47.7	1.8	4.1	0.7
Maximum	129.9	104.8	121.7	128.1	99.0	121.0	42.9	42.5	45.1
95% CI (From)[b]	101.2	89.2	95.6	77.1	66.4	70.2	14.1	14.6	16.0
95% CI (To)[b]	111.4	97.3	106.0	95.6	80.7	87.8	25.8	24.7	27.6

[a]SD: standard deviation.
[b]CI: confidence interval.

Figure 3 shows representative axial MR images taken from the midgland of two patients acquired with (a) and without (b) the expandable ERC and with (c) and without (d) the rigid ERC, respectively. Visually, it is apparent from Fig. 3 that the larger expandable ERC distorted the prostate to a greater degree in both the R/L and A/P dimensions as compared to the smaller rigid ERC. Quantitatively, the prostate was 0.51 cm (12.8%) larger in the R/L dimension when using the expandable coil (4.50 vs 3.99 cm) and only 0.12 cm (3%) larger when using the rigid coil (4.19 vs 4.07 cm). In the A/P dimension, the prostate was compressed by 0.23 cm (7.5%) for the expandable coil (2.84 vs 3.07 cm), while it was negligibly different for the rigid coil, 0.05 cm (2%) (2.51 vs 2.56 cm).

Figure 4 graphically summarizes the A/P (a) and R/L (b) distortions for the rigid (squares) and expandable (circles) ERCs at the base, midgland and apex of the prostate, with the numerical values reported in Table II. Similar to the representative cases shown in Fig. 3, on average the expandable coil caused a significantly larger distortion of the prostate as compared to the rigid coil; compressing the prostate in the A/P direction by 4.1±3.0 mm (mean±standard deviation) vs 1.2±2.2 mm (14.5% vs 4.8%) ($p<0.0001$), and widening the prostate in the R/L direction by 3.8±3.7 mm vs 1.5±3.1 mm (8.3% vs 3.4%) ($p=0.004$). Additionally, the expandable coil consistently caused larger distortions along the S/I length of the prostate (base, midgland and apex of gland) as compared to the rigid coil, with the distortions being significantly larger ($p<0.05$) at all locations except for the A/P dimension at the midgland and the R/L dimension at the base and apex of prostate due to the large variability of

TABLE II. The mean±standard deviation A/P (A) and R/L (B) distortions for the ERCs at the base, midgland and apex of the prostate. Significance between the ERC's is listed, based on Mann-Whitney rank-sum test.

(A) A/P distance decrease between ERC-in versus ERC-out studies (unit is mm)

S/I region of prostate	Type of ERC	Mean (relative change)	Standard deviation
Base	15 rigid cases	1.60 (4.9%)	2.22
($p=0.0115$)	10 expandable cases	4.1 (13.2%)	2.17
Mid	15 rigid cases	1.17 (3.7%)	2.73
($p=0.0593$)	10 expandable cases	3.82 (13.0%)	3.22
Apex	15 rigid cases	0.81 (3.1%)	1.77
($p=0.0163$)	10 expandable cases	4.36 (17.2%)	3.58

(B) R/L distance increase between ERC-in vs ERC-out studies (unit is mm)

S/I region of prostate	Type of ERC	Mean (relative change)	Standard deviation
Base	15 rigid cases	1.45 (4.2%)	3.39
($p=0.0709$)	10 expandable cases	3.76 (7.7%)	3.74
Mid	15 rigid cases	1.61 (4.3%)	3.29
($p=0.023$)	10 expandable cases	3.94 (8.3%)	2.73
Apex	15 rigid cases	1.42 (4.2%)	2.73
($p=0.2852$)	10 expandable cases	3.55 (9.0%)	4.66

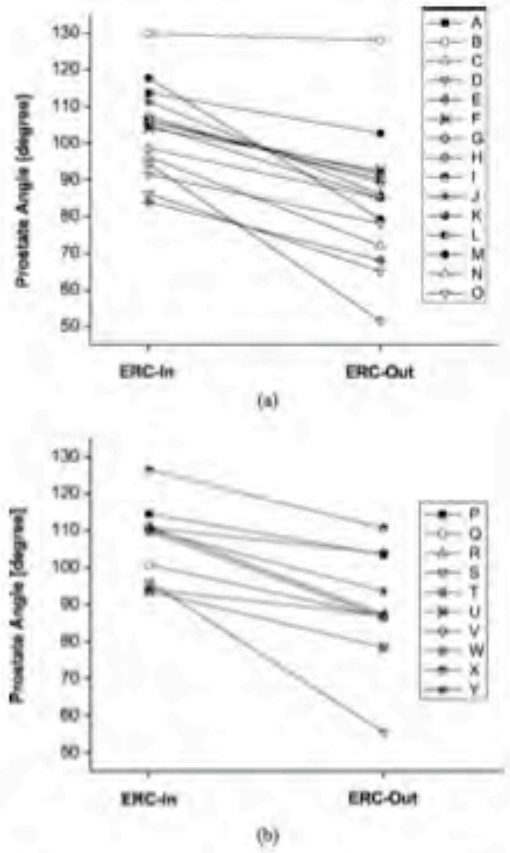

FIG. 2. Summary of the changes in prostate angle between ERC-in and ERC-out studies for the (a) 15 rigid ERC studies (A–O) and (b) 10 expandable ERC studies (P–Y).

these measurements [Figs. 4(a) and 4(b)]. There was no significant difference in the degree of deformation with location (apex, midgland and base) for either ERC.

C. Registration of images acquired with and without ERC

Figure 5 shows representative cases (at the base, midgland and apex of prostate) of the quality of image registration attained after rotations and translations for a rigid coil case [Fig. 5(a)] and an expandable coil case [Fig. 5(b)]. It is visually clear that the registration of images acquired with and without the expandable coil [Fig. 5(b)] is not as good as the registration of images with and without the rigid coil [Fig. 5(a)] due to the larger A/P and R/L distortions caused by the expandable coil. Figure 6 graphically demonstrates the improvement in the similarity index attained using the rigid coil. Quantitatively, the ability to align prostate images acquired with and without ERC was significantly ($p < 0.0001$) better for the rigid coil (SI=0.941±0.008, range from 0.925 to 0.952) than for the expandable coil (SI =0.899±0.033, range from 0.812 to 0.928). In addition, the average difference of SI values calculated by two different observers is 0.0059 with maximum difference of 0.01972. There was no significant difference between the two observers (p value is 0.3525 using Wilcoxon matched-pairs signed-ranks test) in obtaining SI values using rigid image registration between ERC-in and ERC-out MR images. However, each prostate contour for a prostate is different to a certain extent depending on each observer.

IV. DISCUSSION AND CONCLUSION

Recently, there have been a number of published approaches[20–30] for the alignment of high spatial resolution prostate MRI and in some cases MRSI data acquired using an ERC with ultrasound, CT or MR radiation treatment planning images acquired without the use of the ERC or with a differently shaped transrectal ultrasound probe. A majority of these studies utilized a commercially available expandable ERC for MR acquisition.[20,25–30] However, at least two studies[23,24] employed a rigid ERC for the acquisition of the MRI/MRSI data. In this study we demonstrate that while both types of ERCs similarly displace the prostate, the use of a smaller rigid coil significantly reduces the deformation of the prostate, allowing for more accurate image registration using a manual rigid-body approach. The commercially available expandable ERC is larger in size than the rigid alternative ERC. Thus, the independent effects of size and malleability could not be determined in this study.

Specifically, we found that both rigid and expandable ERCs caused the prostate to tilt anteriorly with an average of 18.5° in the sagittal plane. This rotation changed the position of the prostate relative to the surrounding anatomy (pubic symphysis, ischial bone, rectum, bladder and so forth), making the use of external anatomy inaccurate for the registration of the ERC prostate images to treatment planning images. Therefore the approach taken was to use the prostate itself for registration of the imaging data. However, prior to registering the ERC images to the treatment planning images, the ERC images needed to be corrected for the anterior tilt of the prostate.

Neither ERC caused a significant change in the S/I length of the prostate. Hirose *et al.*[31] also observed a negligible deformation (median of 1.5 mm) in the S/I dimension between pre-operative and intraoperative MR prostate images. However, in this study the larger expandable ERC caused both a 3.5-fold larger compression of the prostate in the A/P direction, and a 2.5-fold larger widening of the prostate in the R/L direction as compared to the smaller rigid ERC. In the study by Hirose *et al.*,[31] the expandable ERC caused a mean decrease of 4.9 mm in the A/P dimension and 4.5 mm widening in R/L dimension that were close to the values reported in this study (4.1 and 3.8 mm). A possible explanation for the small difference in gland distortion between the two studies was that the non-ERC images in the study by Hirose *et al.*[31] were acquired with a rectal obturator typically used during brachytherapy to fix the prostate. For both ERCs there was no significant difference in the degree of deformation with S/I location of prostate (apex, midgland and base).

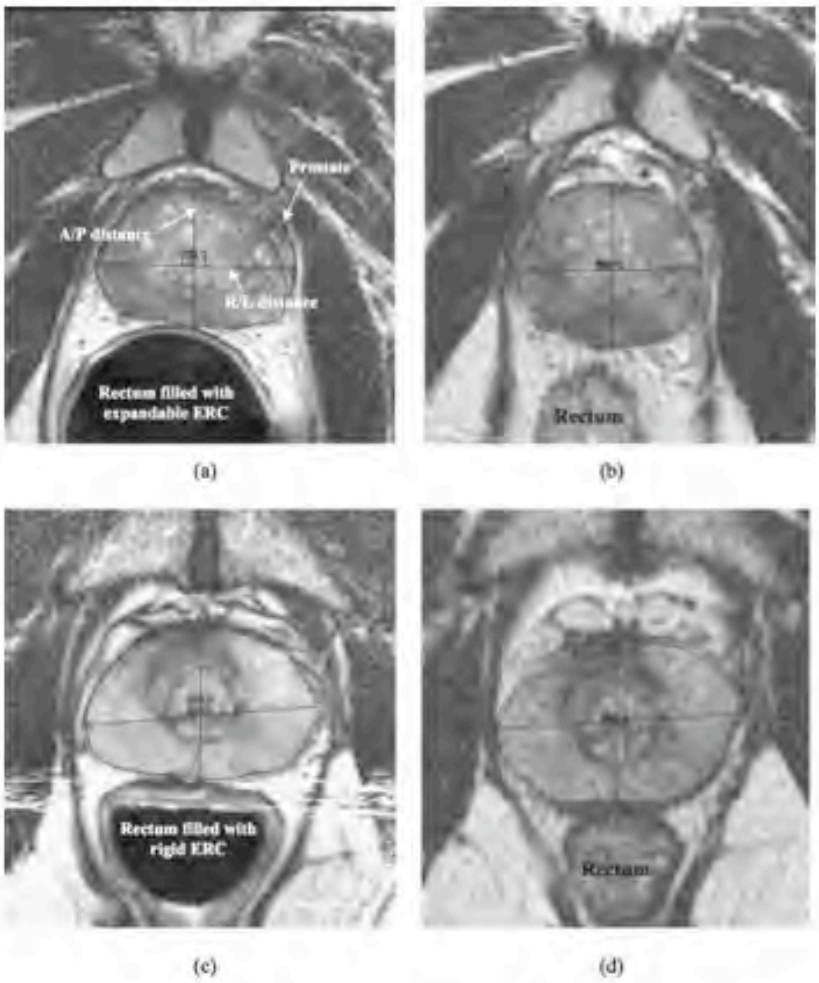

FIG. 3. Representative axial MR images taken from the midgland of two patients acquired with (a) and without (b) the expandable ERC and with (c) and without (d) the rigid ERC, respectively. The R/L distance is 4.50, 3.99, 4.07, and 4.19 cm for (a), (b), (c) and (d), respectively. The A/P distance is 2.84, 3.07, 2.51 and 2.56 cm for (a), (b), (c) and (d), respectively.

The larger distortion of the prostate induced by the expandable ERC resulted in poorer rigid image registration as reflected by a significantly reduced similarity index (0.899 ± 0.033) than that obtained for the rigid coil (0.94 ± 0.008). Although the registration performed in this study involved only manual rotations and translations without any correction for deformation, the mean SI value obtained for the rigid ERC (0.94, 95% confidence interval (CI): 0.937–0.946) was identical to a prior study involving 3D image registration using biomechanical finite element model for the registration of expandable ERC-in and ERC-out images (0.94, 95% CI: 0.89–0.99).[20] However, that study involved subjects scanned in two different positions, supine and lithotomy, which may have also contributed to gland distortion and poorer image registration.

In the current study, there was deformation of the prostate, primarily in the axial plane. Thus, a method to improve upon our current rigid image registration might be to first perform a rigid body rotation as we have done, but then apply a 2D deformable alignment such as B-spline[25] or finite element method[20,24,27] in the axial plane. Further improvements might be obtained with a 3D deformable technique such as in Bharatha *et al.*[20] Such approaches will need to be investigated further and compared to evaluate the benefits and drawbacks of the individual methods for this population.

In this study, three different approaches (described in Section II C) were applied to define the prostate angle. It was shown that there is an insignificant angle difference between ERC-in and ERC-out study for the three approaches in spite of the different prostate angles measured by the three approaches. The impact of the actual prostate angle measured by the three different approaches on prostate deformation and on the 2D manual image alignment was investigated to confirm that the different approaches to measuring the prostate angle did not affect the results. The A/P and R/L dimension deformations and the SI values were measured using all three approaches for prostate B which has the largest discrepancy in prostate angles between three approaches (the angle differences between Approaches I and II are 21.8° for the ERC-in case and 29.1° for the ERC-out case while the

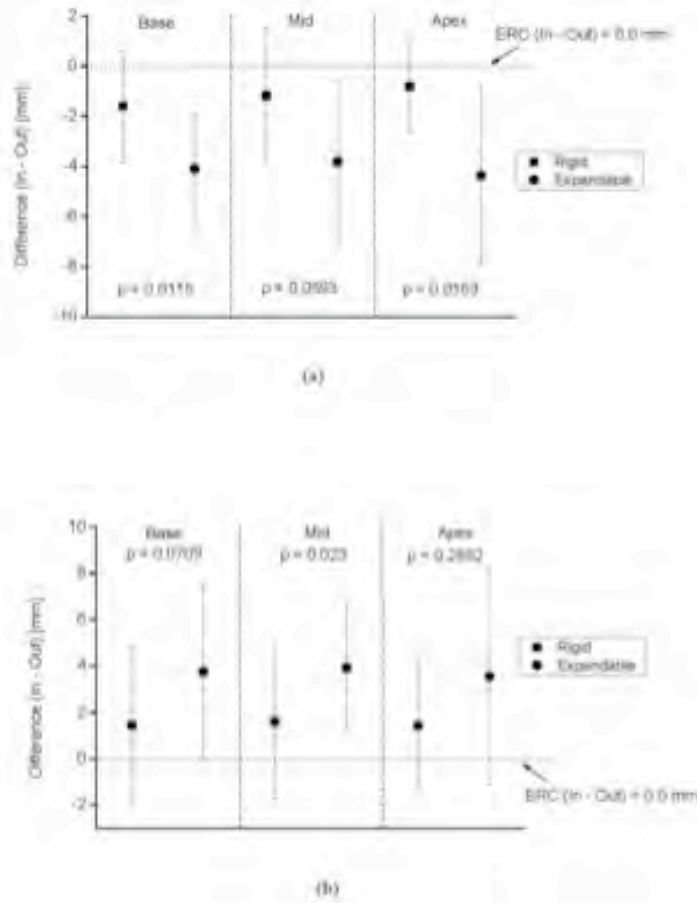

FIG. 4. Graphical summary of the A/P (a) and R/L (b) distortions for the rigid (squares) and expandable (circles) ERCs at the base, midgland, and apex of the prostate. Error bar graphs show mean±standard deviations.

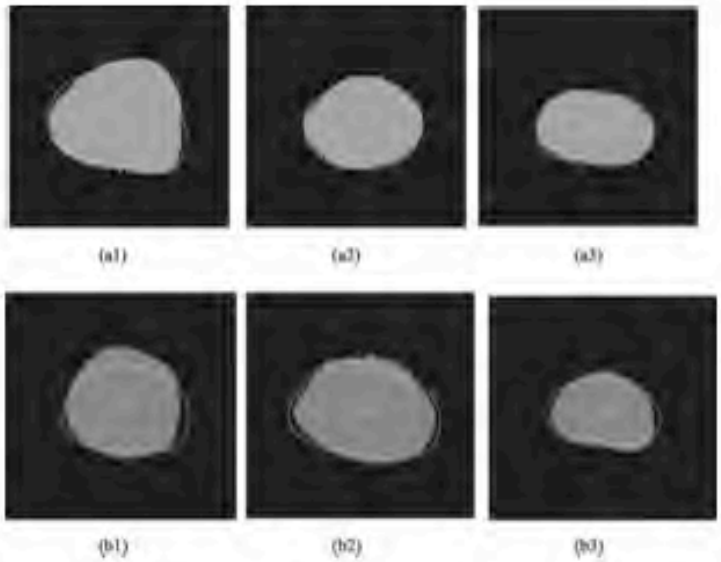

FIG. 5. Representative cases demonstrating the quality of image registration attained after rotations and translation for a rigid coil case [Fig. 5(a)] and an expandable coil case [Fig. 5(b)]. Gray regions are the prostate contours from axial MR images acquired without ERC and white line contours are the prostate contours from axial MR images acquired with ERC. Three axial MR slices were obtained at the base [(a1), (b1)], midgland [(a2), (b2)], and apex [(a3), (b3)] of prostate. The SI values are 0.952 (a) and 0.905 (b).

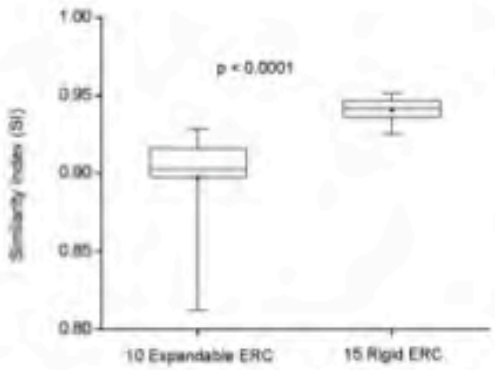

FIG. 6. Comparison of the rigid image registration between rigid and expandable ERC using similarity index (SI). Each parallel bar in the box graph represents minimum, 25, 50, 75 percentiles and maximum values in order and the dot inside the box is the mean value.

angle differences between Approaches II and III are 18.6° (ERC-in) and 22.0° (ERC-out). The mean±standard deviation of A/P and R/L dimension distortions of the three approaches is less than a pixel in size, 0.4±0.4 mm (0.9±0.8%) with a maximum of 1.3 mm (2.5%) for the R/L dimension at the apex of prostate. There is no significant difference in A/P and R/L distortions among all three approaches (p=0.4297 by Friedman test). The SI values are 0.949, 0.959, and 0.953 for Approaches I, II and III, respectively. These values are only 1% or less different and are much less different than the mean values for the rigid (0.941) and expandable (0.899) ERCs. Therefore, the three different approaches to determine the prostate angle do not appear to have significant effects on the determination of A/P and R/L distortions or on the manual alignment SI values.

One concern of the current study is that two of the expandable ERC subjects had unusually large prostates (63.5 and 91.8 cm^3 versus the remaining mean=33.5 cm^3). Calculating expandable ERC distortions and the SI from image registration with or without these cases did not have a significant effect on the results. Without these two subjects, the R/L expansion of the prostate remained the same, at 8.3%, and the A/P compression was slightly and insignificantly less, at 12.6%±2.3 (versus 14.5%±2.4 with all expandable ERC subjects). These distortions were still significantly larger than those with the rigid ERC. When removing the large prostate cases, the mean SI value for the expandable ERCs remained at 0.897, indicating the negligible effect of the prostate size on rigid image registration, at least for these two large prostate cases.

The current study has several limitations due to the manual nature of the registration procedures used, including: (1) the definition of the prostate angle is sensitive to the experience of the reader, (2) the contouring of the prostate gland from images acquired without an ERC had an intrinsic uncertainty due to poorer image quality, and (3) the contouring of the prostate from 2D images acquired with and without an ERC suffers from the fact that the image slices are not at the exact same anatomical locations within the prostate.

In conclusion, both rigid and expandable ERC caused a significant anterior tilt of the superior aspect of the prostate in the sagittal plane and it is important to correct for this rotation when registering images acquired with and without an ERC. The smaller rigid ERC induced significantly less deformation of the prostate in the R/L and A/P dimensions than the larger expandable ERC leading to better rigid image registration of images acquired with and without an ERC.

ACKNOWLEDGMENTS

This work was supported by NIH Grant Nos. CA79980 and CA59897 and DOD Grant No. PCRP030909.

[a]Author to whom correspondence should be addressed. Electronic mail: kim@radonc17.ucsf.edu

[1]M. D. Schnall, R. E. Lenkinski, H. M. Pollack, Y. Imai, and H. Y. Kressel, "Prostate: MR imaging with an endorectal surface coil," Radiology **172**, 570–574 (1989).

[2]H. Hricak, S. White, D. Vigneron, J. Kurhanewicz, A. Kosco, D. Levin, J. Weiss, P. Narayan, and P. R. Carroll, "Carcinoma of the prostate gland: MR imaging with pelvic phased-array coils versus integrated endorectal-pelvic phased-array coils," Radiology **193**, 703–709 (1994).

[3]C. E. Hayes, M. J. Dietz, B. F. King, and R. L. Ehman, "Pelvic imaging with phased-array coils: quantitative assessment of signal-to-noise ratio improvement," J. Magn. Reson Imaging **2**, 321–326 (1992).

[4]J. E. Husband, A. R. Padhani, A. D. MacVicar, and P. Revell, "Magnetic resonance imaging of prostate cancer: comparison of image quality using endorectal and pelvic phased array coils," Clin. Radiol. **53**, 673–681 (1998).

[5]D. J. Gilderdale, N. M. deSouza, G. A. Counts, M. K. Chui, D. J. Larkman, A. D. Williams, and I. R. Young, "Design and use of internal receiver coils for magnetic resonance imaging," Br. J. Radiol. **72**, 1141–1151 (1999).

[6]N. M. deSouza, D. J. Gilderdale, R. Puni, G. A. Counts, and I. R. Young, "A solid reusable endorectal receiver coil for magnetic resonance imaging of the prostate: design, use, and comparison with an inflatable endorectal coil," J. Magn. Reson Imaging **6**, 801–804 (1996).

[7]P. Narayan, D. B. Vigneron, P. Jajodia, C. M. Anderson, M. W. Hollgcock, E. A. Tanagho, and T. L. James, "Transrectal probe for 1H MRI and 31P MR spectroscopy of the prostate gland," Magn. Reson. Med. **11**, 209–220 (1989).

[8]J. Kurhanewicz, A. Thomas, P. Jajodia, M. W. Weiner, T. L. James, D. B. Vigneron, and P. Narayan, "31P spectroscopy of the human prostate gland in vivo using a transrectal probe," Magn. Reson. Med. **22**, 404–413 (1991).

[9]J. Kurhanewicz, M. G. Swanson, S. J. Nelson, and D. B. Vigneron, "Combined magnetic resonance imaging and spectroscopic imaging approach to molecular imaging of prostate cancer," J. Magn. Reson Imaging **16**, 451–463 (2002).

[10]S. J. DiBiase, K. Hosseinzadeh, R. P. Gallapalli, S. C. Jacobs, M. J. Nasland, G. N. Sklar, R. B. Alexander, and C. Yu, "Magnetic resonance spectroscopic imaging-guided brachytherapy for localized prostate cancer," Int. J. Radiat. Oncol., Biol., Phys. **52**, 429–438 (2002).

[11]B. Pickett, E. Vigneault, J. Kurhanewicz, L. Verhey, and M. Roach, "Static field intensity modulation to treat a dominant intra-prostatic lesion to 90 Gy compared to seven field 3-dimensional radiotherapy," Int. J. Radiat. Oncol., Biol., Phys. **44**, 921–929 (1999).

[12]J. Pouliot, Y. Kim, E. Lessard, I. C. Hsu, D. B. Vigneron, and J. Kurhanewicz, "Inverse planning for HDR prostate brachytherapy used to boost dominant intraprostatic lesions defined by magnetic resonance spectroscopy imaging," Int. J. Radiat. Oncol., Biol., Phys. **59**, 1196–1207 (2004).

[13]M. Zaider, M. J. Zelefsky, E. K. Lee, K. L. Zakian, H. I. Amols, J. Dyke, G. Cohen, Y. Hu, A. K. Endi, C. Chui, and J. A. Koutcher, "Treatment planning for prostate implants using magnetic-resonance spectroscopy imaging," Int. J. Radiat. Oncol., Biol., Phys. **47**, 1085–1096 (2000).

[14]M. J. Zelefsky, G. Cohen, K. L. Zakian, J. Dyke, J. A. Koutcher, H. Hricak, L. Schwartz, and M. Zaider, "Intraoperative conformal optimization for transperineal prostate implantation using magnetic resonance spectroscopic imaging," Cancer J. **6**, 249–255 (2000).
[15]"Signa® LX Release 9.1," Chap 6. PROSE Pulse Sequence, 2333956-100 Rev. 0 (05/02), General Electric Company (2002).
[16]J. Kurhanewicz, D. B. Vigneron, H. Hricak, P. Narayan, P. Carroll, and S. J. Nelson, "Three-dimensional H-1 MR spectroscopic imaging of the in situ human prostate with high (0.24-0.7-cm^3) spatial resolution," Radiology **198**, 795–805 (1996).
[17]T. K. Tran, D. B. Vigneron, N. Sailasuta, J. Tropp, P. Le Roux, J. Kurhanewicz, S. Nelson, and R. Hurd, "Very selective suppression pulses for clinical MRSI studies of brain and prostate cancer," Magn. Reson. Med. **43**, 23–33 (2000).
[18]A. A. Schricker, J. M. Pauly, J. Kurhanewicz, M. G. Swanson, and D. B. Vigneron, "Dualband spectral-spatial RF pulses for prostate MR spectroscopic imaging," Magn. Reson. Med. **46**, 1079–1087 (2001).
[19]A. P. Zijdenbos, B. M. Dawant, R. A. Margolin, and A. C. Palmer, "Morphometric analysis of white matter lesions in MR images: Method and validation," IEEE Trans. Med. Imaging **13**, 716–724 (1994).
[20]A. Bharatha, M. Hirose, N. Hata, S. K. Warfield, M. Ferrant, K. H. Zou, E. Suarez-Santana, J. Ruiz-Alzola, A. D'Amico, R. A. Cormack, R. Kikinis, F. A. Jolesz, and C. M. Tempany, "Evaluation of three-dimensional finite element-based deformable registration of pre- and intraoperative prostate imaging," Med. Phys. **28**, 2551–2560 (2001).
[21]M. van Herk, J. C. de Munck, J. V. Lebesque, S. Muller, C. Rasch, and A. Touw, "Automatic registration of pelvic computed tomography data and magnetic resonance scans including a full circle method for quantitative accuracy evaluation," Med. Phys. **25**, 2054–2067 (1998).
[22]C. C. Parker, A. Damyanovich, T. Haycocks, M. Haider, A. Bayley, and C. N. Catton, "Magnetic resonance imaging in the radiation treatment planning of localized prostate cancer using intra-prostatic fiducial markers for computed tomography co-registration," Radiother. Oncol. **66**, 217–224 (2003).
[23]J. Lian, L. Xing, S. Hunjan, C. Dumoulin, J. Levin, A. Lo, R. Watkins, K. Rohling, R. Giaquinto, D. Kim, D. Spielman, and B. Daniel, "Mapping of the prostate in endorectal coil-based MRI/MRSI and CT: a deformable registration and validation study," Med. Phys. **31**, 3087–3094 (2004).
[24]E. Schreibmann, D. Kim, S. L. Hancock, A. Boyer, D. Spielman, B. Daniel, and L. Xing, "Using finite-element method to register endorectal coil-based MRI/MRSI with treatment planning CT images," Int. J. Radiat. Oncol., Biol., Phys. (Abstract) **60**, S592–593 (2004).
[25]M. Kessler, M. Roberson, R. Zeng, and J. Fessler, "Deformable image registration using multiresolution B-splines," Med. Phys. (Abstract) **31**, 1792 (2004).
[26]R. Alterovitz, K. Goldberg, J. Kurhanwicz, J. Pouliot, and I. C. Hsu, "Registering MR with MRS images for HDR prostate treatment using finite element modeling," Med. Phys. (Abstract) **31**, 1791–1792 (2004).
[27]R. Alterovitz, K. Goldberg, J. Kurhanewicz, J. Pouliot, and I. C. Hsu, "Image registration for prostate MR spectroscopy using biomechanical modeling and optimization of force and stiffness parameters," *Proceedings 26th Annual International Conference IEEE Engineering in Medicine and Biology Society* (EMBS, San Francisco, 2004), pp. 1722–1725.
[28]X. Wu, D. Steven, and C. X. Yu, "An iterative method to register MR and ultrasound images for MRSI guided prostate implant planning," Int. J. Radiat. Oncol., Biol., Phys. (Abstract) **60**, S593 (2004).
[29]T. Mizowaki, G. N. Cohen, A. Y. Fung, and M. Zaider, "Towards integrating functional imaging in the treatment of prostate cancer with radiation: the registration of the MR spectroscopy imaging to ultrasound/CT images and its implementation in treatment planning," Int. J. Radiat. Oncol., Biol., Phys. **54**, 1558–1564 (2002).
[30]X. Wu, S. J. Dibiase, R. Gullapalli, and C. X. Yu, "Deformable image registration for the use of magnetic resonance spectroscopy in prostate treatment planning," Int. J. Radiat. Oncol., Biol., Phys. **58**, 1577–1583 (2004).
[31]M. Hirose, A. Bharatha, N. Hata, K. H. Zou, S. K. Warfield, R. A. Cormack, A. D'Amico, R. Kikinis, F. A. Jolesz, and C. M. Tempany, "Quantitative MR imaging assessment of prostate gland deformation before and during MR imaging-guided brachytherapy," Acad. Radiol. **9**, 906–912 (2002).

Class solution in inverse planned HDR prostate brachytherapy for dose escalation of DIL defined by combined MRI/MRSI

(Paper being reviewed, second round)

Yongbok Kim, I-Chow J. Hsu, Etienne Lessard, John Kurhanewicz, Susan Moyher Noworolski and Jean Pouliot*

Yongbok Kim, I-Chow J. Hsu, Etienne Lessard and Jean Pouliot
Comprehensive Cancer Center, Department of Radiation Oncology, University of California, San Francisco, San Francisco, California, USA

John Kurhanewicz and Susan Moyher Noworolski
The Center for Molecular and Functional Imaging, Department of Radiology, University of California, San Francisco, San Francisco, California, USA

The abstract was presented at the 26th Annual Meeting of American Brachytherapy Society in San Francisco, California, USA, on June 2005.

* Corresponding author
Jean Pouliot, Ph.D.
Department of Radiation Oncology, UCSF Comprehensive Cancer Center
1600 Divisadero Street, Suite H1031, San Francisco, CA 94143-1708
Telephone: (415) 353-7190 Fax: (415) 353-9883
E-mail address: jpouliot@radonc.ucsf.edu

Key words: Class solution; Dominant Intra-prostatic Lesion; MR Spectroscopy Imaging; Dose escalation; Inverse planned HDR brachytherapy
Running Title: Class solution in inverse planned HDR prostate brachytherapy
Total number of pages is 30 including 2 tables and 7 figures.

Abstract

Purpose: To establish an inverse planning set of parameters (class solution) to boost dominant intra-prostatic lesion (DIL) defined by MRI/MRSI.
Methods: For 15 patients, DIL were contoured on CT or MR images. A class solution was developed to boost the DIL under the dosimetric requirements of (i) the RTOG-0321 protocol. To determine the maximum attainable level of boost for each patient, five different levels were considered, at least 110%, 120%, 130%, 140% and 150%. The maximum attainable level was compared with the plan without boost using cumulative dose volume histogram (DVH).
Results: DIL dose escalation was feasible for 11/15 patients under the requirements. The planning target volume (PTV) dose was slightly increased, while the DIL dose was significantly increased without any violation of requirements. With further manual adjustment the dose escalation was feasible for 13/15 patients under requirements.
Conclusion: Using a class solution, a dose escalation of the MRI/MRSI defined DIL up to 150% while complying with RTOG dosimetric requirements is feasible. This HDR brachytherapy approach to dose escalation allows a significant dose increase to the tumor while maintaining an acceptable risk of complications.

Introduction

High dose rate (HDR) brachytherapy can safely and accurately deliver radiation dose to prostate cancer. HDR brachytherapy employs catheters inserted directly into the prostate, guided by transrectal ultrasound (TRUS), and adjusts source dwell times along the catheters with a remotely controlled afterloader. Advancements recently made in imaging technology have improved the accuracy and effectiveness of HDR prostate brachytherapy planning. The anatomical information obtained from computed tomography (CT) and magnetic resonance imaging (MRI) images can be displayed along with the dose distribution within the target and the organs at risk (OAR) and significantly improves the control of the dose distribution [10, 14]. The functional imaging information, MR spectroscopic imaging (MRSI) combined with MRI and translated into the planning CT or MRI, was introduced into HDR prostate brachytherapy in order to better identify dominant intra-prostatic malignant lesions (DILs) within the prostate and to escalate the dose on the DIL [16]. Several clinical follow-up studies demonstrated that improved biochemical control, a higher survival rate and a lower risk of complications, is achieved by the dose escalation of prostate cancer with HDR brachytherapy [1, 11-12, 17]. In addition, the development of anatomy-based inverse planning dose optimization for HDR brachytherapy can produce a highly conformal dose profile within one minute, with more than 90% of the prostate volume covered with the prescribed dose and a clinically acceptable sparing of OAR [2, 7-9]. Furthermore, the concept of class solution commonly used in intensity modulated radiation therapy (IMRT) [5, 15, 19] is now available in brachytherapy. The class solution of an inverse planning routine can reduce the variation of treatment plan quality across different users and can dramatically decrease the treatment planning time.

In this study we developed a class solution for boosting MRI/MRS defined DILs in inverse planned HDR brachytherapy of prostate cancer.

Methods and Materials

Patient cohorts

We used data from 15 HDR patients with MRI/MRSI defined DILs (patients A to O). The mean ± standard deviation value of their prostate volume was 43.7 ± 16.3 cc with a range from 28.1 to 86.0 cc. In general, 16 catheters (range from 15 to 18) were inserted using TRUS guided freehand technique to cover the entire prostate. Our current protocol called for a single interstitial implant and two subsequent HDR fractions with each providing 9.5 Gy. The details of the freehand TRUS guided HDR brachytherapy treatment procedure for prostate cancer used at our institution was described in other studies [6, 17].

Definition of the DIL

We overlaid the MRSI data on the axial T2-weighted MR images through post-processing. The resolution of the MRS is 0.3 cc. Each MRSI voxel is scored using a standardized 5-point scale (1- definitely benign, 2- likely benign, 3- equivocal, 4- likely abnormal and 5- definitely abnormal), based on the change of metabolite markers (choline, citrate, creatine and polyamines): elevation of the choline peak and reduction of the citrate, creatine and polyamines peaks in an abnormal MRSI voxel [4]. Based on the combined MRI/MRSI information, DILs were manually contoured on HDR planning axial CT or MR images. A lesion was defined as a DIL (Fig. 1(B)) wherever it contained at least 3 contiguous MRSI validated cancer voxels scored with a 4 or a 5 on combined MRI/MRSI images (Fig. 1(A)).

Dosimetric requirements for a class solution

We developed a class solution that would comply with the dosimetric requirements used in the current RTOG-0321 protocol [3]. The RTOG protocol requires more than 90% of the planning target volume (PTV) to be covered by the prescription dose (9.5 Gy). In this study, PTV was the same as clinical target volume (CTV) and defined by the physician on CT scans. It included the prostate only for T1c-T2b and

the prostate and extra-capsular extension for T3a-T3b, respectively. In addition, each volume of the bladder and the rectum receiving 75% of the prescription dose (7.12 Gy) must be less than 1 cc and the volume of the urethra receiving 125% of the prescription dose (11.87 Gy) must be less than 1 cc. When the bladder and rectum were contoured, the outer most border of the mucosa was included. For the urethra, the outer surface of the Foley catheter was contoured. Throughout the paper, PTV V100[%] is defined as the percent volume [%] of the PTV receiving at least 100% of the prescribed dose while rectum V75[cc] is defined as the absolute volume [cc] of the rectum receiving at least 75% of the prescribed dose.

Anatomy-based inverse planning

Our in house inverse planning routine based in simulated annealing (IPSA) was implemented on the commercial HDR treatment planning system (Plato V14.2, Nucletron, The Netherlands) for evaluation and was clinically/routinely used for HDR brachytherapy at our institution. First, the PTV and OAR are delineated and catheters are digitized on axial CT or MR images. Approximately two thousand dose points are generated on the surface and inside of all the organs (PTVs and OAR). For the surface and inside of all organs, a set of dose constraints is defined as an acceptable dose range (minimum and maximum doses) and weighting factors for penalty values imposed to the minimum and maximum doses. Dwell times were set to zero for all dwell positions outside target and these positions were excluded from the optimization process afterward. Under user-defined dose constraints, IPSA searches the optimal solution (a dwell time combination) through the simulated annealing algorithm to minimize the possibility that any dose point resides outside the acceptable dose range [8]. This process takes less than one minute. Owing to the anatomy-based inverse planning, IPSA can deal with any additional targets and OAR, i.e., seminal vesicles (additional target), DIL boost (target within a target), neurovascular bundle or bulb of penis (OAR outside of the target) and so forth.

Class solution for a plan without boost

Prior to developing a class solution for the DIL-boost plan, a class solution for a plan without a boost was determined. In general, the acceptable dose range is always the same both on the surface and inside of all organs (targets and OAR). The clinically acceptable dose range is from 100% to 150% of the prescribed dose for the PTV and from 100% to 120% for the urethra, which has to be spared from a high dose (hot spot). In our institution, 120% of the prescription dose was used for maximum dose of urethra to ascertain its protection instead of 125%. To other OAR located outside of the PTV such as the bladder and the rectum, ideally no dose should be delivered. Hence, naught is assigned to the minimum dose while a clinically appropriate value such as 50% or 75% of the prescribed dose with its pertinent weighting factor is assigned to the maximum dose. The most important clinical objectives are given the maximum relative weight. The maximum relative weight is given the arbitrary value of 100. All other clinical objectives are given an equal or smaller weight corresponding to their relative importance. For weighting factors to the dose limit, both on the surface and inside of the OAR the same value was applied because any dose should be avoided both on the surface and inside of the OAR simultaneously. However, they were different between on the surface and inside of the PTV. On the surface of the PTV, the weighting factor on the minimum dose should be high enough (the maximum relative weight of 100) to ensure a clinically acceptable PTV coverage by the prescribed dose and the weighting factor on the maximum dose should also be high enough (the maximum relative weight of 100) to avoid contain the dose within the PTV protecting the surrounding normal tissues. Based on our clinical experience, the value of 100 was high enough to penalize the cost function during dwell time optimization when the PTV dose was less than the prescribed dose. Inside the PTV, the weighting factor for the minimum dose was also high enough (the maximum relative weight of 100) that the inside of PTV is fully covered by the prescribed dose. The weighting factor for the maximum dose was reduced to 30 to achieve better conformal dose distribution. This was a dose constraint on the V150 of the PTV and it balanced the compromise between dose

homogeneity and dose coverage. Over the years, our clinical experience demonstrated that a weighting factor of 30 reduces adequately the size of the hot spots while keeping excellent dose coverage. For the urethra, the same weighting factors as the inside of the PTV are used based on previous clinical experience. Regarding weighting factors to the dose limits of the bladder and the rectum, they are well established but sometimes vary depending upon an individual patient. In order to yield a clinically better plan for a patient, a better tradeoff should be made between higher PTV coverage by the prescribed dose and enhanced protection of the bladder and the rectum. Therefore, if the maximum dose limit of the bladder and the rectum is decreased and/or their weighting factor is increased unduly, the bladder and the rectum are overprotected while the PTV coverage is undesirably reduced. On the other hand, if their maximum dose is increased and/or their weighting factor is reduced excessively, the PTV coverage with the prescribed dose can be improved but the rectum and bladder receive an intolerable dose and consequently higher complications are predicted after treatment. Therefore, in this study, by adjusting the maximum dose and the weighting factor of the bladder and the rectum a class solution was determined for a plan without boost under dosimetric requirement.

Class solution for a DIL

A class solution for a DIL was developed based on two perspectives. Primarily the dosimetric requirement should be satisfied. Second, we used 150% of the prescribed dose as the maximum dose escalation goal for the DIL. The maximum dose escalation level (150%) to DIL is the same as the maximum dose desired for the PTV in dwell time optimization even though the dose next to the active dwell positions is higher than 150%.

Prior to examining various levels of a DIL-boost for each patient, the same dose range as the PTV was applied to the DIL to construct a DIL-boost plan equivalent to a plan without a boost. As with the PTV and OAR, the same dose range was used both on the surface and the inside of the DIL. On the surface of the DIL the same weighting factors as the inside of the PTV were employed because the DIL surface has the same clinical importance as the inside of the PTV. In addition, the weighting factor for the minimum dose inside the DIL was the same value as inside the PTV since the DIL should be covered by at least the minimum dose. Finally, for an appropriate weighting factor to the maximum dose limit inside the DIL, seven different values of the weighting factor (from 0 to 30 with 5 points increment) were attempted in the DIL-boost plan equivalent to a plan without boost under dosimetric requirement.

Maximum attainable level of DIL-boost using the class solution

The class solution for the DIL-boost plan was developed by adding a dose constraint for the DIL to the previously obtained class solution for a plan without a boost. By increasing the minimum dose with a 10% increment in the class solution for the DIL-boost plan equivalent to a plan without boost, five different levels of DIL-boost plans were investigated for each patient: 110 – 150, 120 – 150, 130 – 150, 140 – 150, and 150 – 150 (acceptable dose range: minimum – maximum dose in percent relative to the prescribed dose). The highest DIL-boost plan without any violation of requirement was considered as the maximum attainable DIL-boost plan for each patient. For patients reaching certain level of DIL-boost without violation of the requirement, the maximum attainable DIL-boost plan was compared with a plan without boost by analyzing a cumulative dose volume histogram (DVH) of the PTV and the DIL. Additionally, specific dosimetric indices of the PTV (V100[%] and V150[%]) and the DIL (V120[%], V150[%] and V200[%]) were compared between the two plans.

Furthermore, under requirement, the class solution was manually adjusted to achieve the 150 – 150 DIL-boost for those patients for whom the automatic plan was not attainable.

RESULTS

DIL

The mean ± the standard deviation value of the DIL volume in percent relative to the prostate volume was 13.9 ± 7.3% with a range from 2.5 to 31.3% (the absolute DIL volume was 6.3 ± 4.3 cc with range from 1.2 cc to 15.3 cc) for the 15 patients. All patients have one DIL except for patient J who has two DILs. In this study the DIL was always located at the peripheral zone of prostate and its specific location was different depending on each patient: right side, left side or midline in the peripheral zone of the prostate when seen in an axial planning CT or MR image. For example, a DIL was delineated at the right side in the peripheral zone of the prostate in an axial CT image (Fig. 1(b)) acquired for HDR prostate brachytherapy planning. This location was determined from the corresponding MRI/MRSI image (Fig. 1(a)) which demonstrates a validated cancer lesion that comprises five contiguous voxels with a score of 5 (definitively abnormal).

Class solution for a plan without a boost

Table 1 is a class solutions developed for a plan without a boost under requirements. All plans employing the class solution, Table 1, satisfied all dosimetric requirements with a mean PTV coverage (V100[%]) of 92.4% (range from 90 to 94.7%), except for 3 patients (B, J, L). For those patients, the weighting factor to the maximum dose for the bladder and the rectum were tuned to meet requirement. Table 2 shows the change of dosimetric indices corresponding to the change of their weighting factors. For patient B, the bladder and rectum were overprotected with undesirably low PTV coverage (84.54%). The reduction of their weighting factor increased PTV coverage up to 90.26% while keeping their V75[cc] less than 1cc. For patient J, bladder V75[cc] was more than 1 cc. By increasing its weighting factor, bladder V75[cc] was reduced to less than 1cc at the expense of slightly decreased PTV coverage (from 91.29 to 90.46%). For patient L, by decreasing rectum weighting factor, the low PTV coverage (88.81%) was improved to 90.01% while rectum V75[cc] was kept less than 1 cc.

Class solution for a DIL

One out of seven weighting factors to the maximum dose was chosen and a class solution of DIL for the same level of DIL-boost as the PTV was constructed under requirement.

As the weighting factor applied to the maximum dose is increased, the value of DIL V150[%] is reduced due to the heavily imposed penalty value to the maximum dose as shown in Fig 2. In the case of no penalty value (zero weighting factor) applied, a much higher dose can be delivered to the DIL (V150 [%] value is improved in Fig. 2, but the DIL volume receiving more than 150% of the prescribed dose is also undesirably increased). If the rectum and/or bladder are very closely located to the DIL, the dosimetric requirement would be violated: in this study, patients B, E and J violated the bladder dose limit and patients B, F and O violated the rectum dose limit under requirement. Six different DIL-boost plans using its six different non-zero weighting factors (ranging from 5 to 30) applied to the maximum dose showed almost the same protection of the OAR (the same value of OAR dosimetric indices) for all patients. The six DIL-boost plans violated the rectum dose limit for patients F and O and the bladder dose limit for patient J, respectively, under requirement. Without any advantage in the protection of the OAR, the higher weighting factors deteriorated the DIL V150[%] value (Fig. 2). Therefore, the value of 5 was chosen as the best weighting factor and the class solutions of the DIL were achieved on the surface and inside of the DIL (Table 2) for the DIL-boost study.

Maximum attainable level of DIL-boost using the class solution

The class solution obtained by combining a class solution for without-boost plan (Table 1) and a class solution of the DIL (Table 2) was exploited to acquire the maximum attainable level of the DIL-boost for each patient. Under the dosimetric requirement, a DIL-boost was not attainable for four (B, F, J, O) out of

the 15 patients, whereas a certain level of DIL-boost was feasible for the remaining 11 patients (Fig. 3). By averaging all PTV and DIL DVHs of those patients, a mean DVH was generated for the PTV (Fig. 4 (a)) and the DIL (Fig. 5) between the plan without boost and the maximum attainable DIL-boost plan. The averaged PTV DVHs between the two plans were almost the same (< 1% difference) up to 100% of the prescribed dose and they differed slightly in the rest of the dose range (5 – 6% difference between 120% and 160% of the prescribed dose) (Fig. 4(a)). In particular, the PTV coverage by the prescribed dose (Fig. 4(b)) was increased merely by 0.9%, on average, because the prostate was already satisfactorily covered by the prescribed dose (92%) prior to the DIL-boost. The difference was statistically insignificant with p-value of 0.0537 using nonparametric test, Wilcox matched-pairs signed-rank test. The PTV coverage deficiency occurred close to the rectum/bladder because of their dose limit, depending upon the proximity between the PTV and rectum/bladder. The PTV V150[%] was increased by 5.9%,on average, from 34.5% to 40.4% with p-value of 0.0537. On the contrary, the averaged DIL DVH of the maximum attainable DIL-boost plan was noticeably shifted into a higher dose range (from the dashed line (N) to the dotted line (B) in Fig. 5) due to the DIL-boost with a maximum increase of 41.8% at 150% of the prescribed dose (Max.(B-M) of the solid line (B-M) in Fig. 5). Dosimetric indices were significantly improved (p-value < 0.05) for all 11 patients. On average, V120[%] was increased from 83.6% to 99% with p-value of 0.001 in Fig. 6(a), V150[%] was increased from 40.6% to 82.4% with p-value of 0.001 in Fig. 6(b), and V200[%] was increased from 13.2% to 33.2% with p-value of 0.002 in Fig. 6(c). A 150 – 150 DIL-boost was not attainable in eight patients; in four of these (B, F, J and O), no boost was attainable (Fig.3). Out of these 8 patients, the bladder dose limit was violated in patients J and L, while the rectal dose limit under requirement was violated in the remaining six patients. The OAR dosimetric indices were compared in Fig. 7. The relative location of bladder to the PTV varied depending upon patients so that the bladder V75 [cc] was patient-specific in Fig. 7(a). The bladder V75[cc] was increased from 0.46 to 0.53 cc by 0.07 cc, on average. The urethra was so protected in both of plans using IPSA planning that the maximum V125 [cc] was 0.22 cc for DIL boost plan. The urethra V125[cc] was slightly increased from 0.03 to 0.085 cc by 0.055 cc, on average. However, the rectum dose was highly elevated due to the dose escalation to the DIL because the DIL was located in the peripheral zone of prostate next to the border of the rectum. Hence, the rectum V75[cc] was extremely increased from 0.23 to 0.63 cc on average by 0.4 cc with p-value of 0.001 (Wilcox matched-pairs signed-rank test).

By small manual adjustment of a class solution, the 150 – 150 DIL-boost was obtainable without any violation of requirement for 6 out of 8 patients (all except for patients B and J) who did not have an automatically attainable class solution.

DISCUSSION

The class solution in inverse planned HDR prostate brachytherapy for dose escalation of a DIL defined by combined MRI/MRSI is an excellent starting point to explore a customized set of dose constraints to obtain a satisfactory treatment plan for each patient. In this study, a minimum of 150% of the prescribed dose to the DIL (150 – 150 DIL-boost) was feasible for 13 out of 15 HDR brachytherapy plans after small manual tuning of the class solution, complying with dosimetric requirement. However, the 150 – 150 DIL-boost could not be accomplished in cases in which a deficient number of catheters was implanted to cover the whole prostate In HDR brachytherapy, properly locating catheters into the PTV is a prerequisite to obtaining the desired dose distribution with a certain optimization technique such as IPSA. No dose would be delivered to a specific lesion without a catheter. In addition, the proximity of the PTV to the rectum and/or bladder prohibited the 150 – 150 DIL-boost. For example, the volume of prostate B is 86 cc (the largest prostate in this study) and the number of catheters employed implanted was only 17, whereas typically there are 18 for larger prostate. To make matters worse, one of the 17 catheters was implanted outside of the PTV. Also, the rectum is located very close to the prostate. Therefore, the 150 – 150 DIL-

boost under dosimetric requirement could not be attained for prostate patient B, despite manual adjustment of the class solution. For patient J, the size of prostate (51.3 cc) is just larger than average and 18 catheters were well implanted to cover the entire prostate. However, both the rectum and the bladder are located extremely close to the PTV such that the rectal and bladder dose limit of dosimetric requirement were violated for 150 – 150 DIL-boost even though the class solution was manually adjusted.

Under dosimetric requirements, for most patients the DIL-boost increased the DIL dose compared with the plan without boost in Figs. 5 and 6. However, DIL V200[%] was decreased from 14.3 to 14.0% for patient H in Fig. 6(c). For the patient, since the maximum attainable level of DIL-boost was 110% of the prescribed dose as shown in Fig. 3, the most sensitive dose range of DIL due to DIL-boost was 110% and V120[%] was considerably improved from 53.4% to 91.4% in Fig. 6(a) and V150[%] was increased from 29.6% to 39.2% in Fig. 6(b). Such an insufficient DIL-boost in conjunction with the dosimetric requirements on OAR (bladder and rectum dose limit), sometimes, may cause the decreased V200[%] during redistribution of the hot spots in the prostate.

In this study the 150% of the prescribed dose was used for both the minimum and the maximum dose limit of the DIL which means to boost DIL with as least 150% of the prescribed dose as well as to prevent excessive high dose (more than 150% of the prescribed dose) within the DIL simultaneously. This purpose was moderately feasible by relaxing the weighting factor applied to the maximum dose of the inside of the DIL with the value of 5 instead of 30 applied on the surface of the DIL and inside the PTV. As seen as a solid line in Fig.5, the increase of DIL volume due to the DIL-boost has a maximum value at the vicinity of 150% of the prescribed dose: on average, a 41.8% increase in absolute volume from 40.6% to 82.4% at the 150% of the prescribed dose under requirement. This can be interpreted that the most sensitive dose of DIL to dose escalation using the class solution obtained in this study was 150% of the prescribed dose.

The dosimetric requirement of the RTOG-0321 protocol is, to some degree, stringent, and difficult to be accomplished. In particular, satisfying the rectal dose limit (V75[cc] < 1 cc) deteriorated the PTV coverage (V100[%] < 90%) for patient B and J despite manual adjustment of a class solution to achieve a 150 – 150 DIL-boost. Hence, we relaxed the RTOG dosimetric requirement such that the volume of the rectum and the bladder which could receive as much as 75% of the prescription dose was increased to 2 cc. Under the relaxed dosimetric requirement, a class solution was obtained for a plan without a boost. All parameters for the class solution were the same as for the RTOG 0321 case except for the increased maximum dose of bladder and rectum (from 50% to 75% of the prescribed dose) and the increased their weighting factors (from 30 to 40). Due to relaxation of the dose limit to bladder and rectum, the average PTV dose coverage was improved to 95.3% on average (range from 92.9 to 96.9%) compared to 92.4% for RTOG 0321 requirement. The same class solution of DIL was obtained as for RTOG protocol case (weighting factor of 5 to the maximum dose). A certain level of DIL-boost was accomplished using a class solution for all patients (patient B and O for a level of 110%, patient F for a level of 120%, rest of 11 patients for a level of 150%) except for patient J. The plan difference between a plan without boost and maximum attainable DIL boost plan was almost identical to RTOG protocol case with respect to PTV and DIL DVHs. The averaged PTV DVHs between the two plans were almost the same (< 1% difference) up to 110% of the prescribed dose and they differed slightly in the rest of the dose range (5 – 6% difference between 140% and 160% of the prescribed dose). The PTV V100[%] was approximately identical, 95.3% versus 95.5% on average and PTV V150[%] was increased by an average of 5.8%. The DIL V120[%] increased up to 98.8% from 90.5% and the V150[%] was extremely elevated from 46.8% to 85.1% on average and the V200[%] was increased from 15.4% to 34.5% on average. In addition, the most sensitive dose of DIL to the dose escalation was the same as for the RTOG 0321 case, 150% of the prescribed dose (38.8% increase from 43.7% to 82.5%). By small manual adjustment of a class solution, the 150-150 DIL-boost was obtainable for all 4 patients (B, F, J, and O). Therefore, the 150-150 DIL-boost could be attained for more patients under relaxed requirement (11/15 versus 7/15 for the use of the class solution

and 15/15 versus 13/15 after manual adjustment of the class solution). Consequently, a dose escalation of the MRI/MRSI defined DIL up to 150% while complying with either RTOG or relaxed dosimetric requirements is feasible. This class solution may be applicable to other protocol (for example, GEC/ESTRO-EAU recommendations) [7] depending upon its dosimetric requirement.

Conclusion

A class solution was developed for dose escalation of a DIL defined by combined MRI/MRSI in inverse planned HDR prostate brachytherapy. Using the class solution, a certain level of DIL-boost is feasible for some patients under RTOG-0321 dosimetric requirements depending on rectal and bladder doses. While the PTV dose was slightly increased, the DIL dose was noticeable enhanced (on average, 82% of the DIL volume could receive 150% of the prescribed dose) without any violation of the dosimetric requirements. With further adjustment of the class solution, the DIL could be boosted by 150 – 150 for 13 out of 15 patients while satisfying dosimetric requirements. Hence, the established class solution for a DIL-boost is a good starting point to explore a customized HDR prostate brachytherapy plan for a specific patient.

Acknowledgements

The work was supported by a grant from the Department of Defense, Prostate Cancer Research Program (PCRP) 030909.

Table 1(a) Class solution for a plan without boost under RTOG 0321 dosimetric requirement

Volume		Weighting factor to D_{Min} for its penalty	D_{Min} [%]	D_{Max} [%]	Weighting factor to D_{Max} for its penalty
PTV (Target)	ON	100	100	150	100
	IN	100	100	150	30
URETHRA (Organ at risk)	ON	100	100	120	30
	IN	100	100	120	30
BLADDER (Organ at risk)	ON	0	0*	50	30
	IN	0	0*	50	30
RECTUM (Organ at risk)	ON	0	0*	50	30
	IN	0	0*	50	30

ON: on the surface of the contour; IN: inside the volume

D_{Min} [%] and D_{Max} [%]: Minimum and maximum dose in percent with respect to the prescribed dose, respectively.

0*: any number is acceptable for the minimum dose since the weighting factor is null.

Table 1(b) Class solution for a DIL under RTOG 0321 dosimetric requirements

Volume		Weighting factor to D_{Min} for its penalty	D_{Min} [%]†	D_{Max} [%]	Weighting factor to D_{Max} for its penalty
DIL (Target)	ON	100	Vary	150	30
	IN	100	Vary	150	5

D_{Min} [%]† varies depending upon the level of DIL-boost (110, 120, 130, 140 or 150).

Table 2 Manual adjustment of weighting factor to the maximum dose of bladder and rectum and its impact on dosimetric indices for 3 patients in whom a class solution for a plan without DIL boost was not available.

Patient	Manual Adjustment	Weighting factor		Dosimetric index			
		Bladder	Rectum	PTV [%]	Bladder V75[cc]	Rectum V75[cc]	Urethra V125[cc]
B	before	30	30	84.54	0.65	0.07	0.04
	after	25	20	90.26	0.96	0.74	0.03
J	before	30	30	91.29	1.27	0.39	0.14
	after	40	30	90.46	0.99	0.43	0.15
L	before	30	30	88.81	0.40	0.05	0.02
	after	30	25	90.01	0.34	0.13	0.02

References

[1] Astrom L, Pedersen D, Mercke C, Holmang S and Johansson KA. Long-term outcome of high dose rate brachytherapy in radiotherapy of localised prostate cancer. Radiother Oncol 2005;74:157-161.

[2] Hsu IC, Lessard E, Weinberg V and Pouliot J. Comparison of inverse planning simulated annealing and geometrical optimization for prostate high-dose-rate brachytherapy. Brachytherapy 2004;3:147-152.

[3] Hsu IC, Shinohara K, Pouliot J, Purdy J, Michalski J and Ibbott GS. RTOG-0321 protocol: Phase II trial of combined high dose rate brachytherapy and external beam radiotherapy for adenocarcinoma of the prostate. (Radiation Therapy Oncology Group, Philadelphia, 2004) http://www.rtog.org/

[4] Jung JA, Coakley FV, Vigneron DB et al. Prostate depiction at endorectal MR spectroscopic imaging: investigation of a standardized evaluation system. Radiology 2004;233:701-708.

[5] Khoo VS, Bedford JL, Webb S and Dearnaley DP. Class solutions for conformal external beam prostate radiotherapy. Int J Radiat Oncol Biol Phys 2003;55:1109-1120.

[6] Kim Y, Hsu IC, Lessard E, Vujic J and Pouliot J. Dosimetric impact of prostate volume change between CT-based HDR brachytherapy fractions. Int J Radiat Oncol Biol Phys 2004;59:1208-1216.

[7] Kovacs G, Potter R, Loch T et al. GEC/ESTRO-EAU recommendations on temporary brachytherapy using stepping sources for localised prostate cancer. Radiother Oncol 2005;74:137-148.

[7] Lachance B, Beliveau-Nadeau D, Lessard E et al. Early clinical experience with anatomy-based inverse planning dose optimization for high-dose-rate boost of the prostate. Int J Radiat Oncol Biol Phys 2002;54:86-100.

[8] Lessard E and Pouliot J. Inverse planning anatomy-based dose optimization for HDR-brachytherapy of the prostate using fast simulated annealing algorithm and dedicated objective function. Med Phys 2001;28:773-779.

[9] Mahmoudieh A, Tremblay C, Beaulieu L et al. Anatomy-based inverse planning dose optimization in HDR prostate implant: a toxicity study. Radiother Oncol 2005;75:318-324.

[10] Martin T, Kolotas C, Dannenberg T et al. New interstitial HDR brachytherapy technique for prostate cancer: CT based 3D planning after transrectal implantation. Radiother Oncol 1999;52:257-260.

[11] Martinez AA, Gonzalez J, Spencer W et al. Conformal high dose rate brachytherapy improves biochemical control and cause specific survival in patients with prostate cancer and poor prognostic factors. J Urol 2003;169:974-979; discussion 979-980.

[12] Martinez AA, Gustafson G, Gonzalez J et al. Dose escalation using conformal HDR brachytherapy improves outcome in unfavorable prostate cancer. Int J Radiat Oncol Biol Phys 2002;53:316-327.

[13] Menard C, Susil RC, Choyke P et al. MRI-guided HDR prostate brachytherapy in standard 1.5T scanner. Int J Radiat Oncol Biol Phys 2004;59:1414-1423.

[14] Mott JH, Livsey JE and Logue JP. Development of a simultaneous boost IMRT class solution for a hypofractionated prostate cancer protocol. Br J Radiol 2004;77:377-386.

[15] Pouliot J, Kim Y, Lessard E, Hsu IC, Vigneron DB and Kurhanewicz J. Inverse planning for HDR prostate brachytherapy used to boost dominant intraprostatic lesions defined by magnetic resonance spectroscopy imaging. Int J Radiat Oncol Biol Phys 2004;59:1196-1207.

[16] Pouliot J, Lessard E and Hsu IC. Advanced 3-D planning. In: Thomadsen B, Rivard M. and Butler W, editors. Brachytherapy physics. 2nd Edition, Madison: Med. Phys. Publishing. 2005; 393-414.

[17] Vicini FA, Kestin LL, Martinez AA. Use of conformal HDR brachytherapy for management of patients with prostate cancer: optimizing dose escalation. Tech Urol 2000;6:135-145.

[18] Xia P, Lee N, Liu YM et al. A study of planning dose constraints for treatment of nasopharyngeal carcinoma using a commercial inverse treatment planning system. Int J Radiat Oncol Biol Phys 2004;59:886-896.

Figure Captions

Figure 1. (a) Axial MR image and MRSI voxel grid with its spectral scores at the midgland of prostate I. (b) HDR brachytherapy planning axial CT image at the midgland of prostate I shows contours of the target, urethra, rectum and DIL manually drawn based on Fig. 1(a). Sixteen catheters were implanted to cover the entire target volume, seen as black dots.

Figure 2. Percent volume of the DIL receiving at least 150% of the prescribed dose (V150[%]) of 7 DIL-boost plans with different weighting factors for its penalty value imposed to the maximum dose (150% of the prescribed dose) of the DIL in comparison with a plan without boost (Ref.) under dosimetric requirements. Parallel bars represent the maximum, 75, 50, 25 percentile and minimum values and the black dot represents the mean value.

Figure 3. Under dosimetric requirement, the maximum attainable level of a DIL-boost for 15 patients

Figure 4. For 11 patients who allowed a certain level of DIL-boost, the averaged target DVHs (a) are compared between the plans without boost and with the maximum attainable DIL-boost plan. Several dosimetric indices of PTV are also compared between the two plans for the target (V100 [%] – (b) and V150[%] – (c))

Figure 5. For 11 patients who allowed a certain level of DIL-boost, the averaged DIL DVHs are compared between the plans without boost and with the maximum attainable DIL-boost plan.

Figure 6. For 11 patients who allowed a certain level of DIL-boost, several dosimetric indices of DIL are compared between the plans without boost and with the maximum attainable DIL-boost plan (V120[%] – (a), V150[%] – (b) and V200[%] – (c)).

Figure 7. For 11 patients who allowed a certain level of DIL-boost, dosimetric indices of OAR are compared between the plans without boost and with the maximum attainable DIL-boost plan (Bladder V75[cc] – (a), Rectum V75[cc] – (b) and Urethra V125[cc] – (c)).

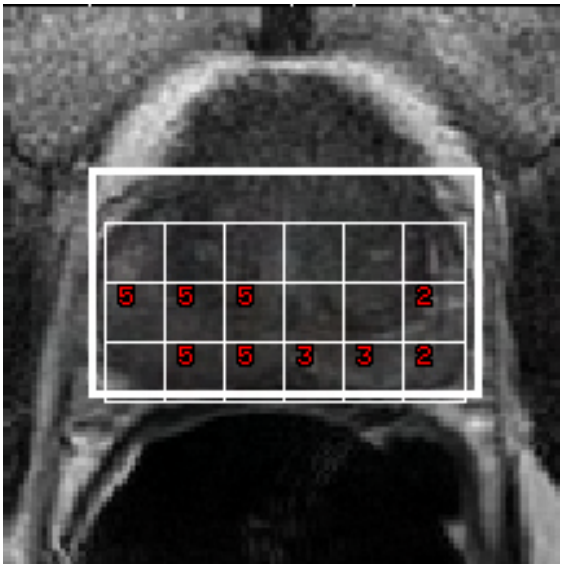

(a)

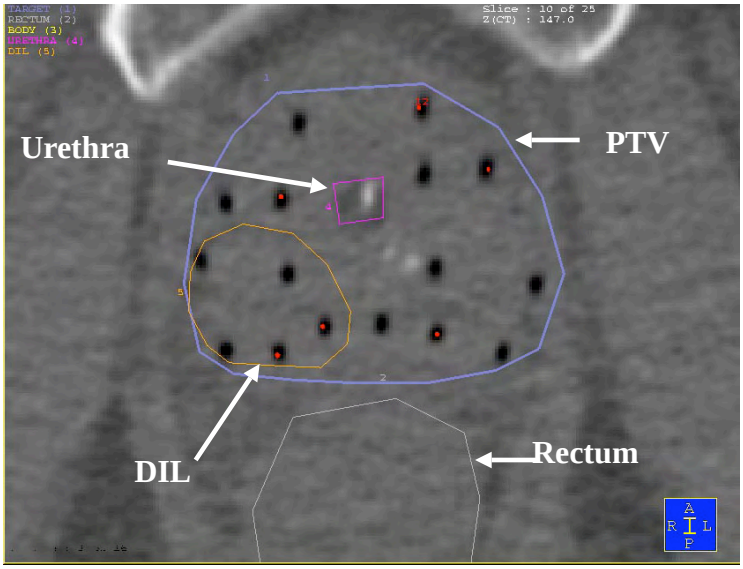

(b)

Figure 1. Kim *et al.* Class solution in inverse planned HDR prostate brachytherapy

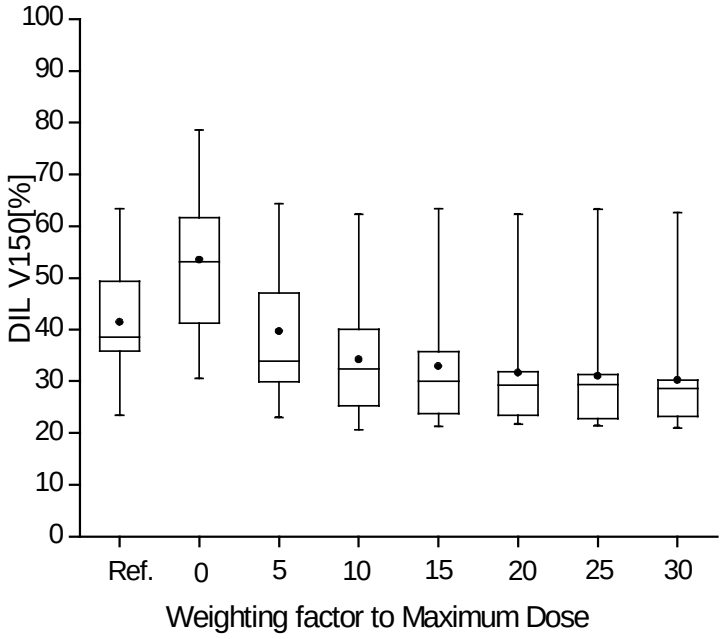

Figure 2. Kim *et al.* Class solution in inverse planned HDR prostate brachytherapy

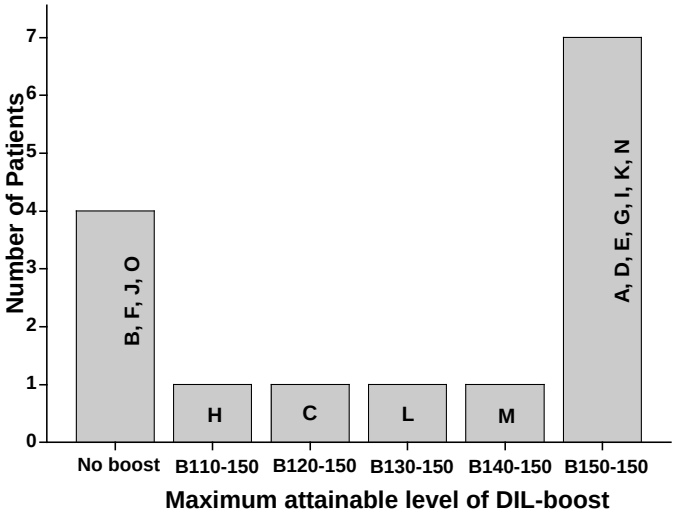

Figure 3. Kim *et al.* Class solution in inverse planned HDR prostate brachytherapy

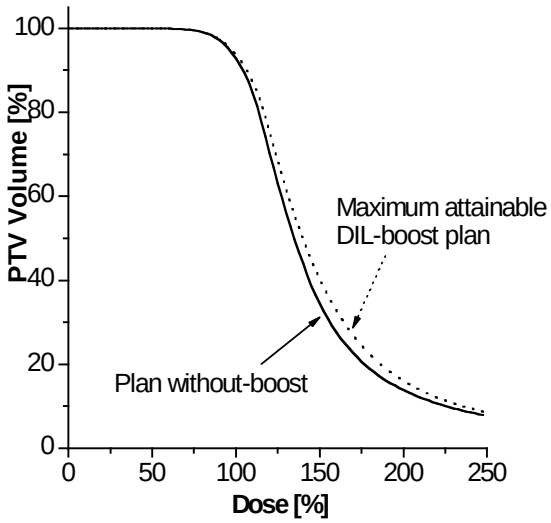

(a)

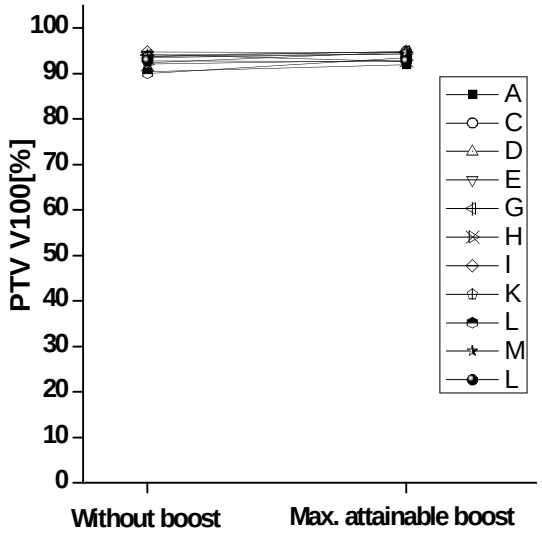

(b)

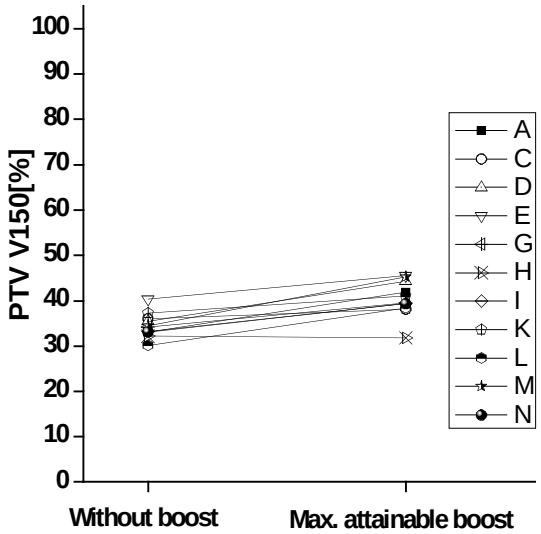

(c)

Figure 4. Kim *et al.* Class solution in inverse planned HDR prostate brachytherapy

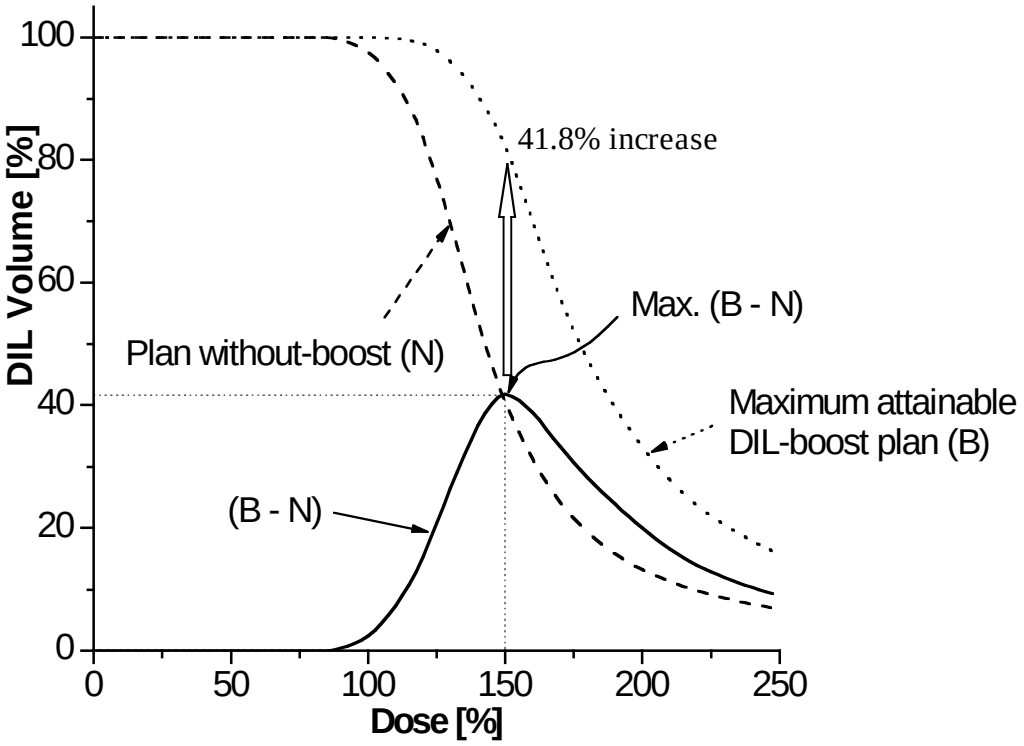

Figure 5. Kim *et al.* Class solution in inverse planned HDR prostate brachytherapy

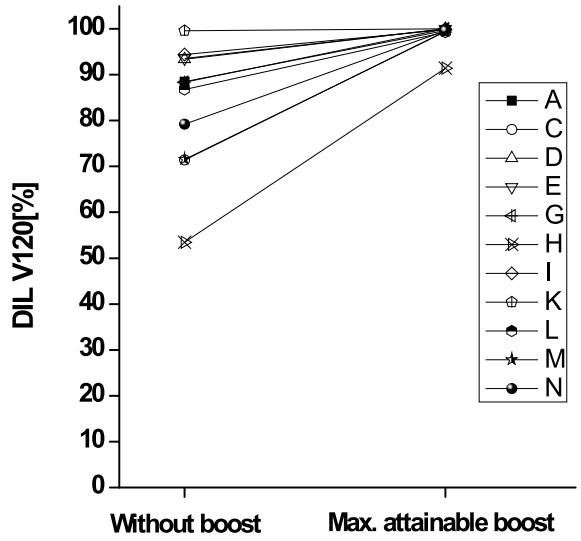

(a)

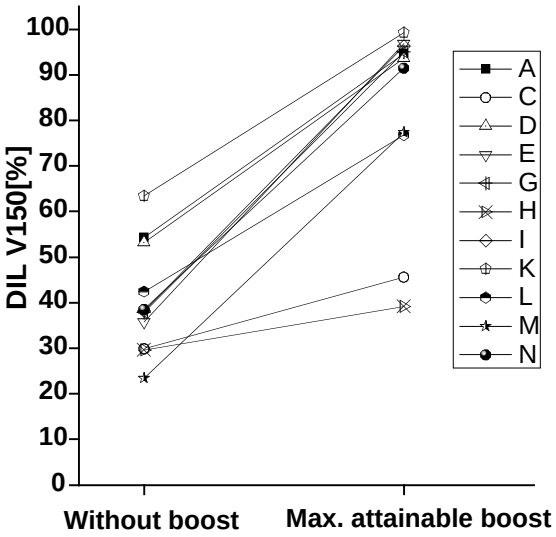

(b)

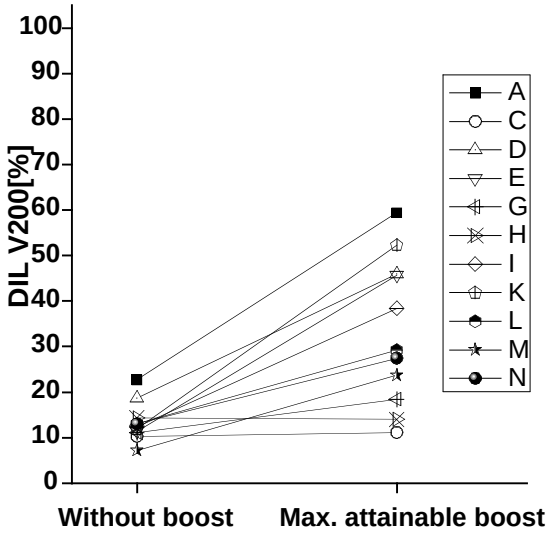

(c)

Figure 6. Kim *et al.* Class solution in inverse planned HDR prostate brachytherapy

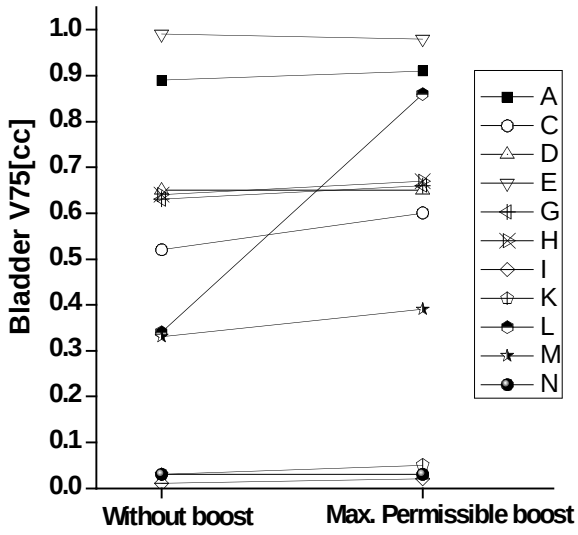

(a)

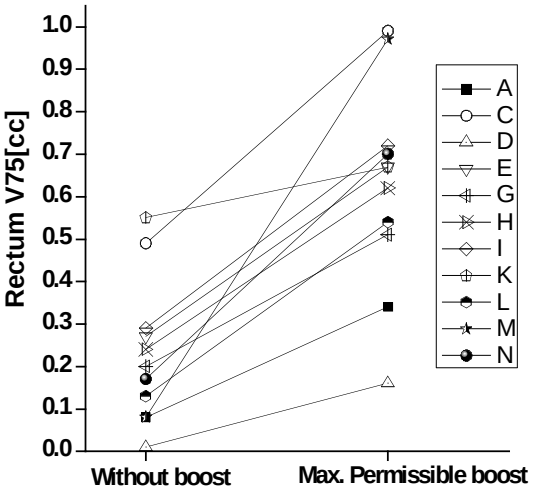

(b)

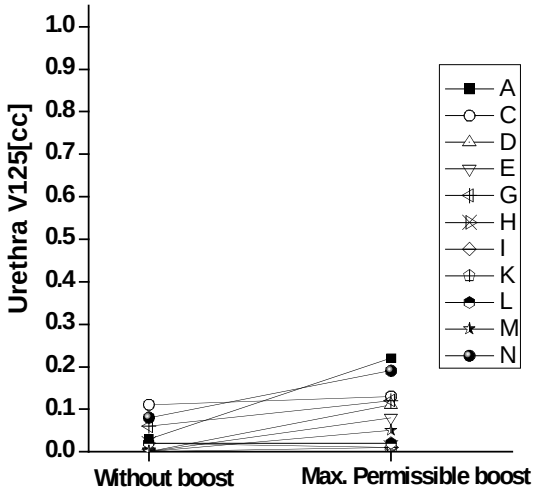

(c)

Figure 7. Kim *et al.* Class solution in inverse planned HDR prostate brachytherapy